RDU130390

ELECTROMAGNETIC BRAKING EFFECT FOR POWER STEERING SYSTEM

GIGIH PRIYANDOKO

RESEARCH VOTE NO:
RDU130390

Faculty of Mechanical Engineering
Universiti Malaysia Pahang

2016

ABSTRACT

This research describes the study of vibration suppression by using eddy current as a suppression agent on a power steering system. Vibration occurs due to some factors such as engine vibration, road surfaces, vibration direction, tire characteristics, suspension design and steering devices. The objective of this study is to investigate the voltage induced effect on vibration suppression occurred at power steering system using eddy current braking. The equipment involve are accelerometer, data acquisition (DAQ), electric motor, transformer, aluminium disc and Voltage regulator. Position of the accelerometer was placed at the steering wheel and aluminium disc. Based on the result for frequency domain, in a normal condition, the level of vibration amplitude produce is 0.2348mvolt. while, after voltage was apply to power steering system lowest vibration suppression at steering column (aluminium disc) is 0.166mVolt with 2 mm air gap opening using 48 Volt power supply. For steering wheel, in a normal condition is the level of vibration is 0.2251mVolt. After voltage was applied to power steering system, the lowest vibration suppression at steering wheel is 0.1836mVolt using 96 Volt of voltage induced. Based on the experimental result, increasing voltage induced managed to reduce vibration on power steering system since the electromagnetic braking force using eddy current increase which act as the vibration suppression agent.

Key researchers: Gigih Priyandoko
Mohd Shahrir bin Mohd Sani
Fadhlur Rahman bin Mohd Romlay

E-mail : *gigih@ump.edu.my*
Tel. No.: 09 424 6219

Vote No.: RDU130390

ABSTRAK

Kajian ini menerangkan penindasan getaran dengan menggunakan arus pusar sebagai ejen penindasan pada sistem stereng kuasa. Getaran berlaku disebabkan oleh beberapa faktor seperti getaran enjin, permukaan jalan, arah getaran, ciri-ciri tayar, reka bentuk penggantungan dan peranti stereng. Objektif kajian ini adalah untuk menyiasat voltan teraruh kesan ke atas penindasan getaran berlaku pada sistem stereng kuasa menggunakan brek semasa pusar. Peralatan yang melibatkan adalah pecutan, perolehan data (DAQ), motor elektrik, transformer, cakera aluminium dan pengatur voltan. Kedudukan pecutan itu diletakkan di stereng dan cakera aluminium. Berdasarkan kepada keputusan untuk domain frekuensi, dalam keadaan normal, tahap hasil getaran amplitud 0.2348mvolt. manakala, selepas voltan adalah terpakai kepada sistem stereng kuasa penindasan getaran terendah di kolum stereng (cakera aluminium) adalah 0,166 mVolt dengan jurang udara 2 mm membuka menggunakan bekalan kuasa 48 Volt. Untuk stereng, dalam keadaan normal adalah tahap getaran adalah 0,2251 mVolt. Selepas voltan telah digunakan untuk sistem stereng kuasa, penindasan getaran terendah pada stereng adalah 0,1836 mVolt menggunakan 96 Volt voltan teraruh. Berdasarkan keputusan eksperimen, meningkatkan voltan teraruh berjaya mengurangkan getaran pada sistem stereng kuasa sejak daya brek elektromagnet menggunakan peningkatan arus pusar yang bertindak sebagai ejen penindasan getaran.

TABLE OF CONTENTS

Page

LIST OF FIGURE

CHAPTER 1

INTRODUCTION

1.1 INTRODUCTION

Nowadays, vehicle, structures, building and anything that related in engineering are very important to consider as good and safe. Safety is very important in engineering field in order to increase the rank and standard of engineering, same goes to the technology and achievement reached by engineering.

Steering system is very important for vehicles operation system. Hydraulic power steering and electronic power steering are the example of the power steering system. It functions to rotate the front wheel tyre in the desire direction through the input from driver's steering. Normally power steering was controlled by hydraulic pump for hydraulic power steering or electric actuator for electric power steering when controlled energy to steer the vehicle. When the steering is steered, response torque tends to return the wheel sequence to the apply force. More torque applies to steering wheel, will allow more fluid by the valve to cylinder and increase force applied to move the wheel. Basically, large vehicle required steering effort especially during low speed power steering is to assist the vehicle in turning steering wheel. Most of the power steering system in vehicle have an engine-driven hydraulic and a hydraulic actuator. Electronic power steering is called drive by wire or steer by wire. Electric Power Steering (EPS) is a complete electronic system of steering exertion is reduced by put on the output since an electric motor directly toward the steering system.

It provides feedback of force acting to the front wheel and give moving sense to the wheel. Steering wheel use valve to control fluid flow to cylinder. Hydraulic power steering system is powered by engine using belting to transmit power from the engine to the hydraulic pump. It been started by high pressure operational oil flowing pass through the power steering hose joined among the steering gear box and hydraulic oil pump. The part of power steering consists of hydraulic oil pump, power steering hose, gear box steering, return hose, oil reservoir, heat protector, front axle cross member and steering column shaft assembly.

Sometimes vibration occurs at the steering wheel. This is because of the speeding up level and spectral content of steering wheel vibration depend on some factors such as engine vibration, road surface, direction of vibration, tyre characteristics, design of suspension and steering device of vehicle. The frequency of vibrational energy at the steering wheel can extent up to 300 Hz (Giacomin et al., 2004), the steering wheel and column vibration mode can generate high resonance peaks point in the steering wheel power spectrum at frequencies in range of 20 to 50 Hz (Pottinger et al., 1986).

According to Maxwell's law, an electric field produces when there is a time-varying of magnetic field. This will cause eddy currents to pass through in the electric conductor material. For the example eddy current flows through the resistance of conductor material, these currents dissipate energy. Hence, causing drag force on the conductor that is related to its velocity relation to the magnetic field. The device hence functions such as a viscous damping element.

Nowadays, eddy currents have widely remained used in home electric purposes, non-contact measurement equipment, and braking systems for high-speed train. The benefits of using eddy current brake systems (Wiederick et al., 1987) because it is contactless devices, therefore causing in semi-permanent devices. This contactless device can reduce vibration, no friction and environmental friendly. Takagi et al. have review on thin plate bend by using analytically and experimentally in magnetic field. Their research used excessive current of several hundred amperes of an electromagnet to produce the magnetic field forces. From the research by CSA Engineering Inc. a system of magnetic tuned mass damper for a spaceship solar collection and a magnetically damped separation mount for spaceship consignment. (Matsuzaki et al., 1997) suggested the idea of a different vibration control system which the vibration of the partly magnetised beam is suppressed with the forces from electromagnetic source. They implemented the analysis of vibration suppression using the thin beam and the two magnetised parts exposed to an impulsive force to validate the system effectiveness.

An electromagnetic damper was derived by Graves et al using mathematical models. The derivation refers to electromagnetic field movement and electromagnetic transformer devices. These two devices will be presented to compare theoretical. Due to the movement of close circuit electromagnetic filed device produces current that pass through a stationary magnetic field. A time-varying in magnetic field will generate an

electromagnetic field within a stationary conducting circuit using transformer electromagnetic field device. Recently, investigation from Kwak et al. found that eddy current damper can be effective method for vibration suppression based on proved experimental results and effect of using eddy current damper on cantilever beam. Nevertheless, derivation is not too detailed on eddy current damping and a simple of electromagnetic theory used in its place.

When a moving conductive material passes in between stationary electromagnetic pole, it will produce magnetic drag force. Hence speed of conductive material will decelerate automatically. Phenomenon of eddy current braking happen when changing of magnetic flux induce eddy current in conducting material while dissipate energy to produce drag force. Changing in magnetic flux induces eddy currents on conductor. These currents dissipate energy in the conductor and generate drag force.

Eddy current breaking concept has been suggested to improve notation stability of the dual-spin satellite system (Haines, 1973) and as a vibration suppression of spacecraft (Tossman, 1971). Recently eddy current braking concept is used in dynamometers used in bicycle, motor cycle and other automotive transport. The advantages of magnetic drag force are working to improve several damping components for operational without requirements of any electronic devices or power supplies. Some applications of eddy current resistance are electromagnetic braking, stationary exercise cycling bike and electromagnetic shock absorber.

1.2 PROBLEM STATEMENT

Current power steering systems operate on hydraulic pump. The system was controlled by the hydraulic pump connected with belting to the engine pulley. The previous power steering system can be easily vibrating when car move at a high speed or decelerate. At high speed steering wheel become very light to turn and easy to lost control. This situation very risky for drivers and passenger. There are many important keys that cause this problem such as hydraulic pump, engine vibrate, road surface condition, fluid flow in steering hose, tire balancing, tie rod end loose and even the alignment of tire is not right. Nowadays, cars are provided with an electronic power

steering with high cost system to stop the vibration on the steering wheel and give the artificial drive comfort when turn the steering wheel.

In order to enhance the steering performance for medium price vehicle at lower cost, electromagnetic damping system will be introduced to the current hydraulic power steering system. The electromagnetic damping will act as an active damper system to control the hydraulic steering position and steering wheel will feel heavier than normal one. The uses of electromagnetic damper on steering shaft is a low cost equipment that have the same function as the current technology that being used in current cars to stop the steering vibration.

1.3 OBJECTIVES

The aims of the project are set as follows:

i. To investigate the factors contributed to vibration on power steering system at middle or low segment car.
ii. To explore the effect on vibration suppression system of low segment car using eddy current braking effect on power steering system.

1.4 SCOPE OF STUDY

Scopes of the study are:

i. Power steering used in this experiment is Mitsubishi RVR Hydraulic Power Steering
ii. Suppressed vibration by using eddy current braking system.
iii. Testing Method using Modal Analysis technique
iv. Design 2D and 3D drawing
v. Tri axial Accelerometer was used to measure vibration response, and measure three dimension axes.
vi. Rotational speeds of electric motor are in range of 500 until 1400 round per minute.

vii. Voltage apply in to eddy current are 48Volt until 144Volt with 24Volt increment, air gaps of 2mm, 4mm and 6mm, different number of eddy current use and speed of rotation motors is fixed.

1.5 PROJECT OVERVIEW

This project has been divided into five chapters. Chapter 1 indicated the introduction of the project.

In Chapter 2 briefly explain on experiment set up, experiment procedure, vibration measurement and ending with discussion. This chapter also discuss on methods have been used to fabricate the power steering test rig and preparation of testing methods to find the highest vibration location at steering system. Once finish testing method preparation, continue on apply eddy current damping force in order to suppressed vibration that applied to power steering column. After that run the experiment for vibration measurement to analyse excitation vibration at steering column and steering wheel of the system.

Chapter 3 presents the conclusion from the results obtains from this project and some recommendation to improve for the future research.

CHAPTER 2

VOLTAGE INDUCED EFFECT FOR VIBRATION SUPPRESSION USING EDDY CURRENT ON POWER STEERING SYSTEM

2.1 ABSTRACT

This paper describes the study of vibration suppression by using eddy current as a suppression agent on a power steering system. Vibration occurs due to some factors such as engine vibration, road surfaces, vibration direction, tire characteristics, suspension design and steering devices. The objective of this study is to investigate the voltage induced effect on vibration suppression occurred at power steering system using eddy current braking. The equipment involve are accelerometer, data acquisition (DAQ), electric motor, transformer, aluminium disc and Voltage regulator. Position of the accelerometer was placed at the steering wheel and aluminium disc. Based on the result for frequency domain, in a normal condition, the level of vibration amplitude produce is 0.2348mvolt. while, after voltage was apply to power steering system lowest vibration suppression at steering column (aluminium disc) is 0.166 mVolt with 2 mm air gap opening using 48 Volt power supply. For steering wheel, in a normal condition is the level of vibration is 0.2251 mVolt. After voltage was applied to power steering system, the lowest vibration suppression at steering wheel is 0.1836 mVolt using 96 Volt of voltage induced. Based on the experimental result, increasing voltage induced managed to reduce vibration on power steering system since the electromagnetic braking force using eddy current increase which act as the vibration suppression agent.

2.2 INTRODUCTION

Some of noise and vibration of a vehicle are caused by the power steering system. Excitation vibration of power steering is affected by the engine itself and it will transfer pass through along steering shaft toward steering wheel (Latif and Rus, 2014, Balcı and Gündoğdu. 2013, Kachare and Bimleshkumar. 2013). The vibration in motor usually in periodic and simultaneously toward the shaft rotation which occurred at low

hand-wheel velocity and low frequency level (Balcı at. al., 2014). Steering system usually involved of a steering wheel handle and a steering shaft column. Both of these main components are disposed to vibration that produced from road condition and engine excitation itself. The most important purposes of the power steering system that needs to transfer the static loads from driver toward the system, therefore leading to a series of problem. Power Steering is an important subsystem in automobiles system. The function of power steering is to rotate the front wheel tire in the required direction through the input force from the steering wheel. Power steering consists of two types which are hydraulic power steering and electronic power steering. The hydraulic power steering is controlled by a hydraulic pump while electronic power steering was controlled by an electric actuator. When the steering was steered, response torque tends to return the wheel sequence to the applied force. If more torque applies to steering wheel, than more fluid allow by the valve to cylinder and more force was applied to moving the wheel. Frequency level of excitation energy at the steering wheel can reach up to 300 Hz (Giacomin, at. al., 2004), steering shaft and steering wheel vibration mode can generate high resonance peaks in the steering wheel at frequencies in the range of 20 until 50 Hz (Pottinger at. al., 1986). The previous research from (Reynolds and Angevine, 1977) has studied about the mechanical response toward the steering wheel system to sinusoidal translational vibration in the frequency range of 20 to 500 Hz when holding a steering wheel. From the research Reynolds et al concluded that the position of the arm only gives a slight reaction on the impedance of the hand opposite with tested frequency limitation. However grip tightness and hand pressure affected the excitation vibration at higher frequencies that exceed 60 Hz. So once grip technique was applied, a linear system could be considered by the hand–arm system.

An electromagnetic braking force that comes from the relations between magnetic flux and eddy current. While the movement of conducting material through a stationary magnet, the motion had been slow down by magnetic drag force. Changing in magnetic field will induce eddy current in the conductive material. This current will eliminate energy in the conductor and produce drag force (Lee and Park, 1998). These electromagnetic resistances for steering system will increase the steering feel and vibration by creating a braking effect resistance or drag force to oppose the rotational direction while torque is applied to the steering wheel (Baharom at. al., 2011). Based on early research of the electromagnetic braking system, it was found that aluminium is the

best conductor material to use as the conductor brake disc compared with copper and zinc. The reactions and eddy current effect on aluminium are more effective than copper and zinc. The motion had been decelerating by a magnetic drag force produced during a moving conducting material pass through a permanent magnet or vice versa. So that to decrease the excitation vibration and increase the steering controlled performance, comfort on hydraulic power steering system, electromagnetic eddy current braking system can be applied. As the speed of vehicle increase, more efficient power steering system required to ensure safety and reliability of the vehicles. When the contact friction of the tire is reduced with high velocity driving, the steering effort is weak and the steering stability becomes worse. To prevent this, either the assisted steering effort should be reduced or the steering wheel should be held tight.

Vehicle stability control systems that sustain the stability of the vehicle in order to maintain a dynamic safety protection system (Yusop at. al., 2013). The achievement of electromagnetic brakes much more reasonable for other equipment compared with other retarders (Yusoff at. al., 2011). The conventional brakes can be used less often and hence practically certainly not grasp high temperatures. In addition, electromagnetic brake can avoid the unsaved situation that can occur from the sustained used exceed its ability to dissipate heat. It does not need to use cooling system. The eddy current braking system does not influence the engine component efficiency, such as exhaust and hydraulic brakes. The electromagnetic brakes also provide good control assist. One of the uses could be effective change when the magnet relative toward the moving conductor, to increase the net rate between both devices and instigate a higher damping force. Other active control approaches can use electromagnets to suppress vibrations. If a number of researches continue to develop towards eddy current damping, this kind of damper for sure will find a way of typical applications and will change the commercial market of the automotive industry. The advantages of using an electromagnetic braking system because it is non-mechanical, no moving parts that will not produce friction energy. The research from SAE the Engineering Society for Advancing Mobility Land, Sea Air and Space said that vibration can feel at the steering wheel. The source of steering excitation vibration was generated by fluid pump and engine transferred pass through the steering shaft to the steering wheel. Therefore, the idea of this project will use the application of drag force or resistance generated by electromagnetic braking of eddy current to suppress vibration on the current power steering system. The non-

contact braking and resistance generated will reduce vibration, increase the handling and control stability, and improve the driving comfort. It will become another solution in order to overcome the problem occurred in lower and medium cost segment vehicles.

This paper presents electromagnetic braking using eddy current as a suppression agent on a power steering system. The objective of this study is to investigate the voltage induced effect on vibration suppression occurred at the power steering system using eddy current braking. The position of the accelerometer was placed on the steering wheel and aluminium disc. Based on the experimental result, increasing voltage induced managed to reduce vibration on the power steering system since the electromagnetic braking force using eddy current increase which act as the vibration suppression agent.

2.3 EXPERIMENTAL SETUP

This experimental setup involves the hardware measurement device such as accelerometers. The test was done to get the acceleration signal from power steering system at different part. A National Instrument DAQ measurement device was used to change analogue input into the signal input to the computer. The accelerometer sensor was located at a critical point of vibration excitation level. In addition, to obtain maximum accuracy of accelerometer reading, the sticky or grease gum for accelerometer was used to attach the accelerometer to the steering shaft. The steering shafts are divided into several points to get the different reading at different points. For preliminary study, the impact hammer was used to produce excitation force toward the steering shaft column. The force sensor provides to produce a measurement of the frequency and amplitude content of the energy content stimulus that is transmitted to a test object. In order to maintain a measurement of the object's structural response due to the hammer blow, an accelerometer is used together with the impact hammer. To suit the condition of the item in testing, a variety of tips outfitted with each hammer allow the energy content of the force impulse to be tailored. National instrument DAQmx is used with multi-channel and analysis software. It is able to resolve a variety of mechanical properties that related to an understanding on structural behavioural of an

object characteristic. Items analysed including mode shape, transfer characteristics, resonance detection and beam structural health.

The steering shaft vibration is then suppressed by using eddy current braking system. Steering shaft is placed between eddy current poles (eddy current pole place right and left side of steering shaft). Another test rig is used for eddy current system to suppress excitation vibration of steering shaft. Figure 1 shows the overview experiment setups of main equipment's are computer, accelerometer and National Instrument Data Acquisition. The data acquisition system of National Instrument (NI) has been used. NI-cDAQ 9171 which is a 1 slot USB consist of four input channel been connected to the tri axial accelerometer of (number series 3 axis). This data acquisition system and accelerometer will be configured using Measurement and Automation Explorer (MAX) software of National Instrument (NI). Then the Dasylab will synchronize the measurement setup with the MAX itself. For the preliminary study the sensor was placed to the steering shaft and test rig. After determine the highest location of vibration, this experiment continues to focus on steering wheel and aluminium disc representing the steering column. The aluminium disc is placed in between of four eddy current laminated steel facing each other. The holder is used to hold the eddy current in a fixed position when conducting the experiment. The position of accelerometer need to place at fixed position on steering wheel and aluminium disc to get better signal result.

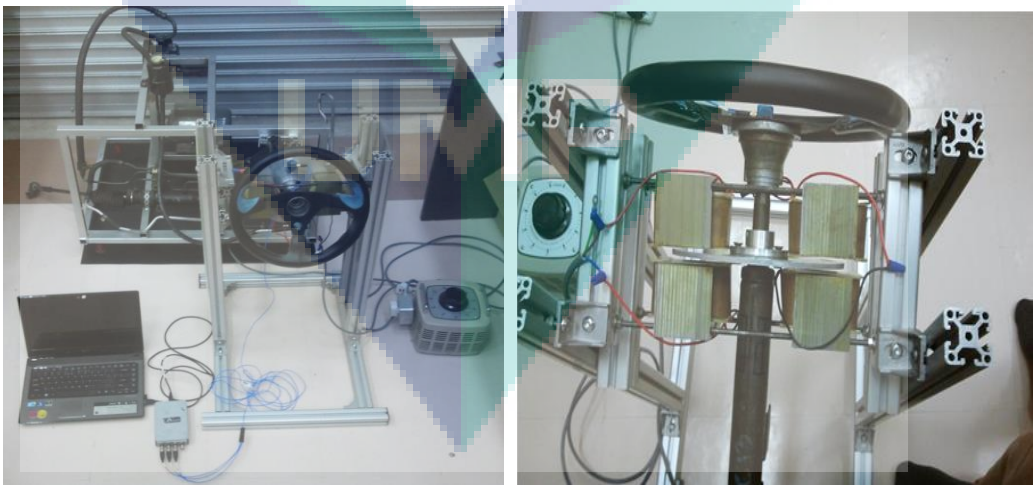

Figure 1. Full view for experimental setup.

As a safety precaution, check the voltage regulator controller before switch on the power supply, voltage regulator is limit until 144 volts to control voltage source of eddy current to avoid it from overheated. Make sure all of the wires connect properly to the eddy current and voltage regulator to avoid from short circuit. The accelerometer place perpendicular to steering shaft. Special wax is used on the accelerometer surface to assure the accelerometer does not move during system is running. The position of accelerometer is placed at the high vibration level to get the better signal input. The research from (Reynolds and Soedel, 1972), they placed small accelerometers in their experiment at two different points along the steering shaft column and measured the value of mechanical response to handle that caused translational vibration. Vibration at frequencies above 100 Hz was limited to the fingers and hand.

2.4 RESULTS AND DISCUSSION

Data from the experiment which is, time domain were converted into frequency domain signal. Time domain was integrated two times to get graph amplitude versus time displacement graph. The result obtained is a power spectrum in the frequency domain, time domain and displacement graph signals that has been analysed. To analyse data Matlab software was used to plot the graph. Figure 2 show, the position of tri-axial accelerometer at steering wheel and aluminium disc. From the figure, the motion of pulley is rotational that will transfer the movement into x-axis, y-axis and z-axis. So, the highest of vibration amplitude in each axis need to be determined first. Figure 3-5 shows that, the time domain, frequency domain and displacement graph for x-axis, y-axis and z-axis, respectively. For the top graph is x-axis, middle graph is y-axis and the rest graph is the z-axis respectively. As illustrate in all the graphs, the vibration signal at x-axis is dominant compare to the y-axis and z-axis. This is due to the rotational movement of pulley and electric motor apply on the test rig, which means force acting through in all axis as shown in Figure 2.

Figures 2 until 16 shows the signal value at voltage 48V until 144V of 2mm air gap for different number of poles at aluminium disc, the value acceleration at x-axis, y-axis and z-axis. Figures 17-31 shows the frequency domain for different number of pole at steering disc. While, Figures 32-49 shows the frequency domain graph for different

number of air gap at aluminium disc and steering wheel. Thus, from the value at all axis, study on frequency domain analysis only considers at highest vibration signal which is x-axis and y-axis. Lastly are mean amplitude graph with increasing voltage induce, from Figures 50-53.

Figures 2-5 shows the results from the first experiment. Total frequency and magnitude of signal recording time are presented. The power steering is starting to vibrate after the switch is turned on and using block average module to get the four times signal average of frequency domain is collected by Dasylab software. This to ensure the signals measured are stable throughout the data collecting process. This condition applied for all the tests.

2.4.1 Number of Poles at Aluminium Disc

Figures 2-4, show the frequency domain graph with power supply of 48Volt. From Figure 2 the mean amplitude value before apply eddy current is 0.2348mVolt and the lowest mean amplitude is 0.166mVolt using 2 pole eddy current. Figure 3 representing the y-axis graph with highest mean amplitude before apply eddy current is 0.2817mVolt after apply eddy current the lowest mean amplitude is 0.2782mVolt using 2 poles of solenoid. While at z-axis as show in Figure 4, highest mean amplitude before apply eddy current is 0.1836mVolt while the lowest mean amplitude is 0.1504mVolt by using 3 pole of laminated steel.

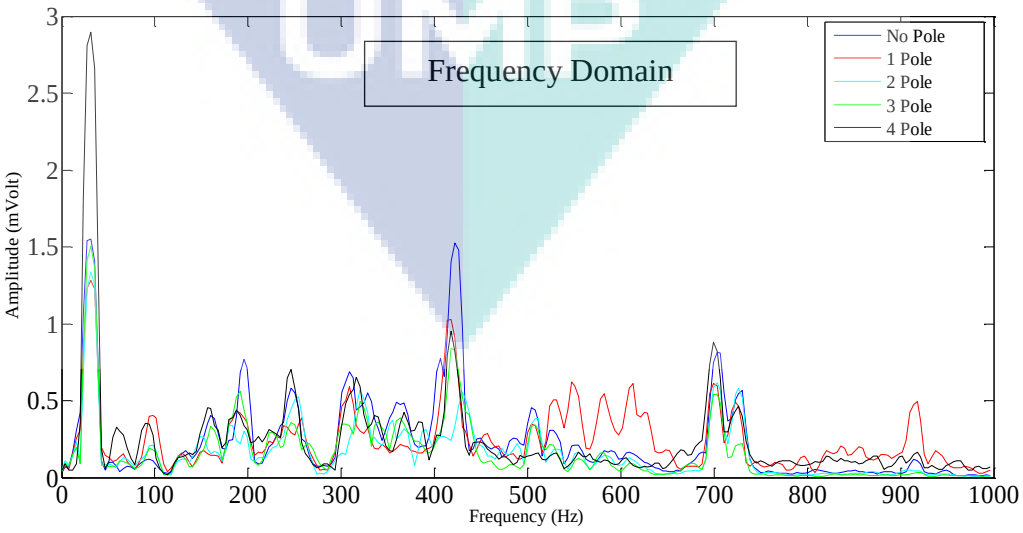

Figure 2. Frequency domain graph for x-axis using 48Volt power supply

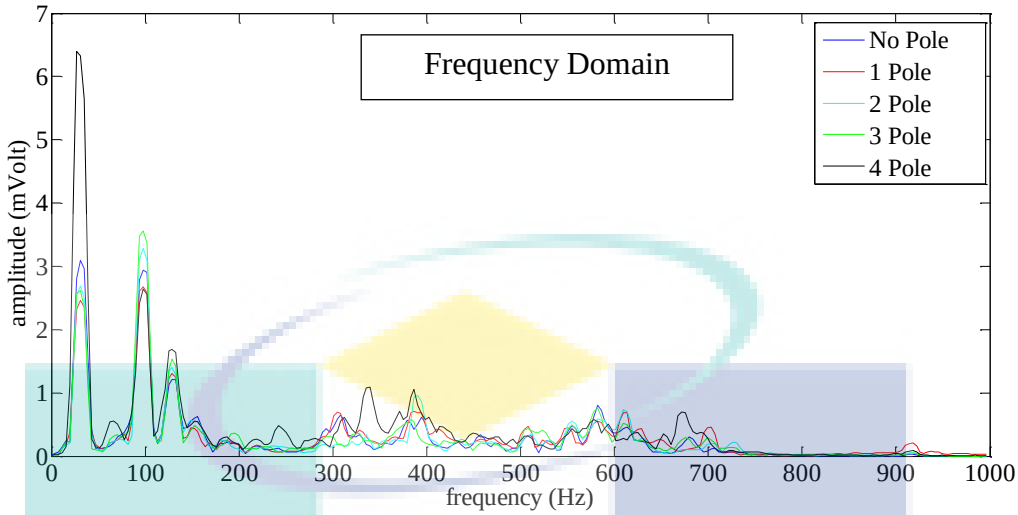

Figure 3. Frequency domain graph of y-axis at 48 Volt power supply

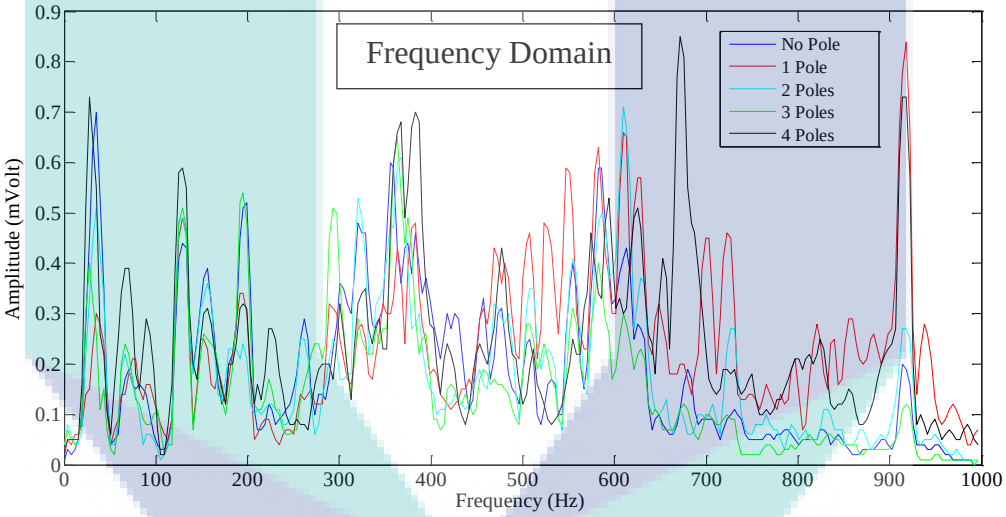

Figure 4. Frequency domain graph for z-axis using 48Volt power supply

Figures 5-7 show the frequency domain graph with power supply of 72 Volt. From Figure 5 the highest amplitude value before apply eddy current is 1.543mVolt at 27.34 Hz and the lowest amplitude is 1.198mVolt at 27.34Hz. After apply eddy current, the lowest frequency is 421.9 Hz with amplitude of 0.424mVolt using 2 eddy current. Figure 6 representing the y-axis graph with highest amplitude before apply eddy current is 3.06mVolt at 31.25Hz after apply eddy current the lowest amplitude is 2.34mVolt at same frequency when using 2 eddy current. While at z-axis in Figure 7, highest amplitude before apply eddy current is 0.7mVolt at frequency 35.16. the lowest amplitude is 0.16mVolt at 35.16Hz.

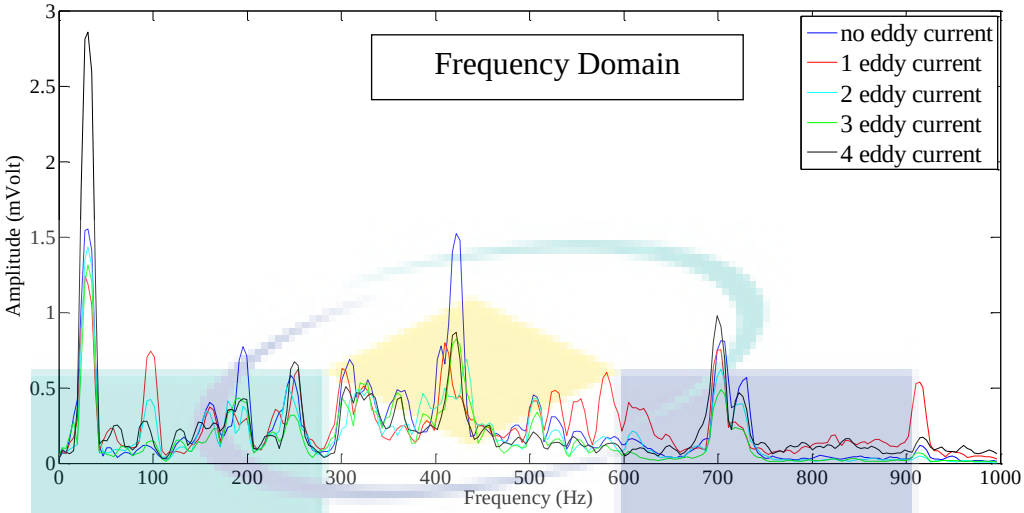

Figure 5. Frequency domain graph for X-axis using 72Volt power supply

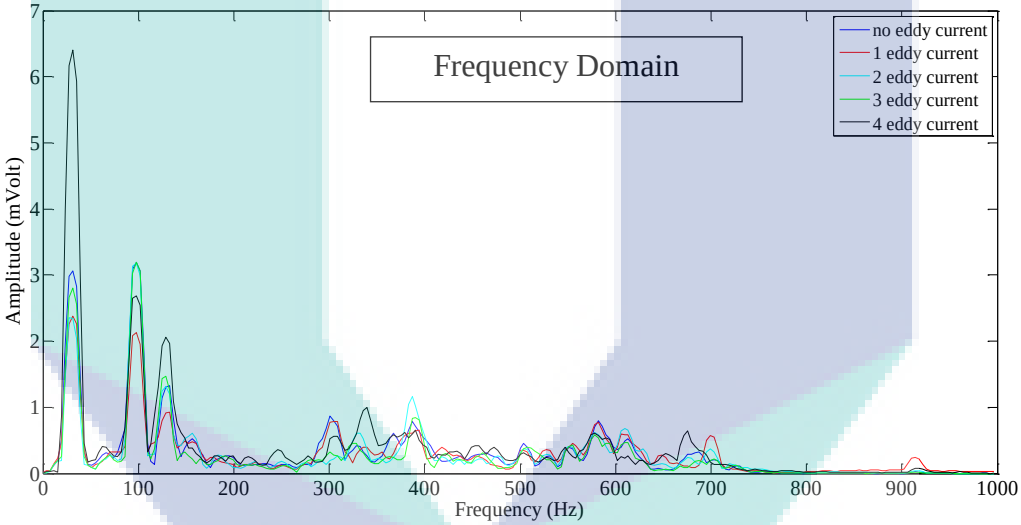

Figure 6. Frequency domain graph for y-axis using 72Volt power supply

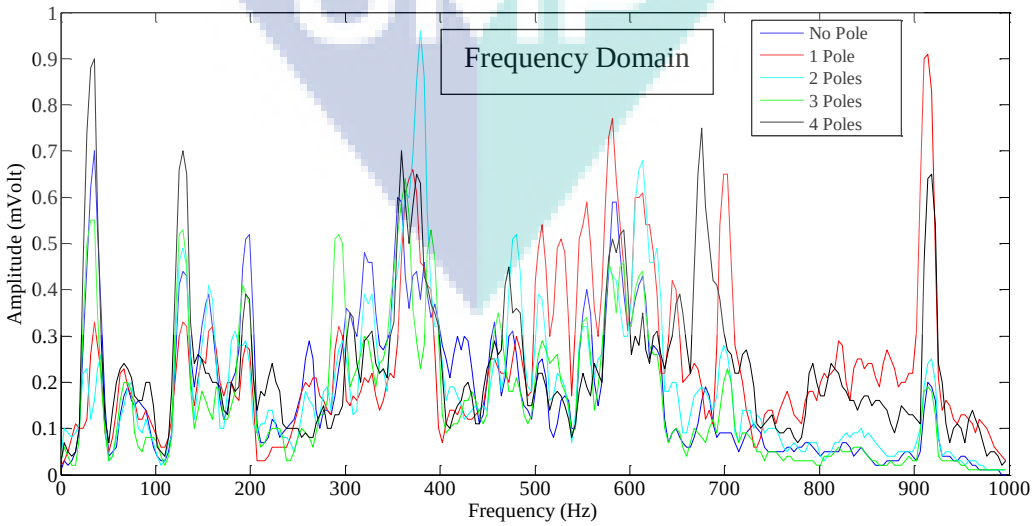

Figure 7. Frequency domain graph for z-axis using 72Volt power supply

Figures 8-10 show the frequency domain graph with power supply of 96 Volt. From Figure 8 the highest amplitude value before apply eddy current is 1.552mVolt at 31.25 Hz. After apply eddy current, the lowest amplitude is 1.317 mVolt at frequency 31.25Hz using 2 eddy current. The second highest amplitude at x-axis is 1.525 mVolt at frequency 421.9 Hz, after apply eddy current the lowest amplitude value is 0.6306mVolt at 425.8Hz. Figure 9 representing the y-axis graph with highest amplitude before apply eddy current is 3.06mVolt at 31.25Hz after apply eddy current the lowest amplitude drop is 2.46mVolt at same frequency when using 2 eddy current. While Figure 10 show z-axis graphs, the highest amplitude before apply eddy current is 0.7mVolt at frequency 35.16 after using eddy current the lowest amplitude drop to 0.41mVolt at 35.16Hz.

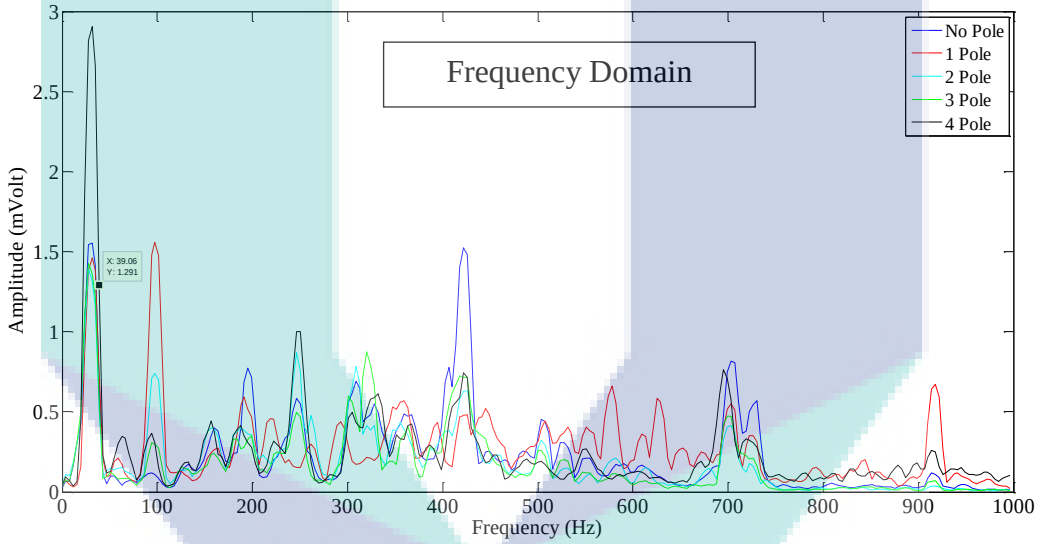

Figure 8. Frequency domain graph for x-axis using 96Volt power supply

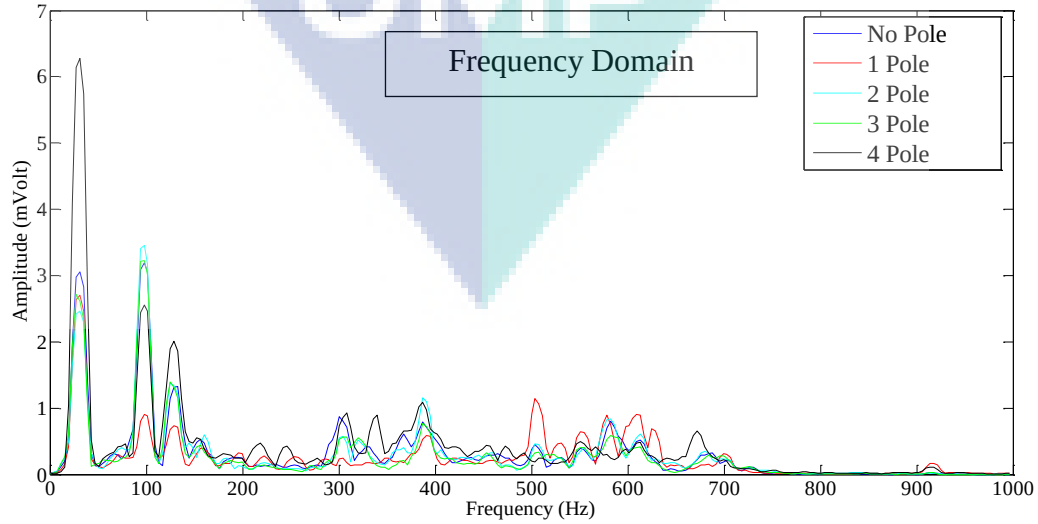

Figure 9. Frequency domain graph for y-axis using 96Volt power supply

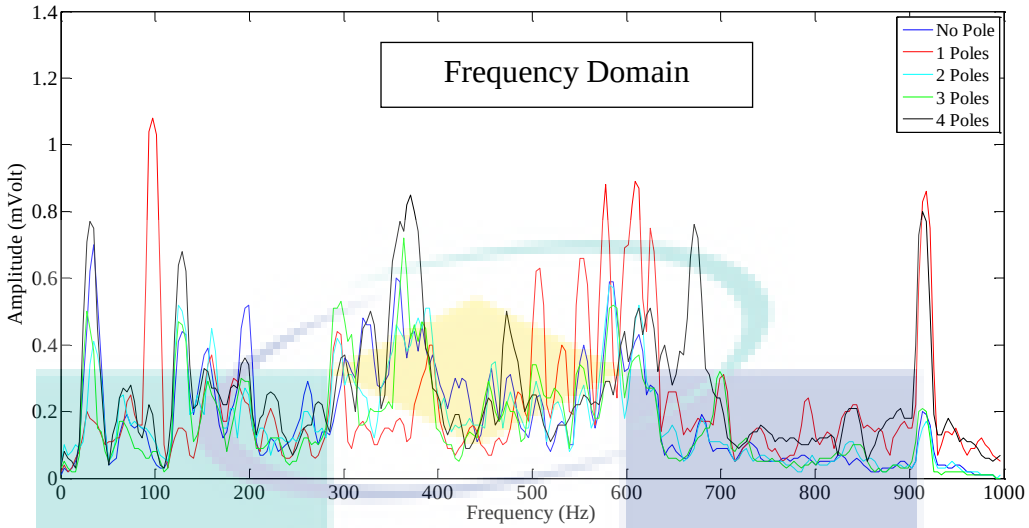

Figure 10. Frequency domain graph for z-axis using 96Volt power supply

Figures 11-13 show the frequency domain graph with 120Volt power supply. From Figure 11 the highest amplitude value before apply eddy current is 1.552mVolt at 31.25 Hz. After apply eddy current, the lowest amplitude is 1.354mVolt at frequency 31.25Hz using 2 eddy current. The second highest amplitude at x-axis is 1.525mVolt at frequency 421.9 Hz, after apply eddy current the lowest amplitude value is 0.5435mVolt at 425.8Hz. Figure 12 representing the y-axis graph with highest amplitude before apply eddy current is 3.19mVolt at 97.66Hz after apply eddy current the lowest amplitude drop is 2.59mVolt at same frequency when using 4 eddy current. Second highest amplitude before apply eddy current is 3.06mVolt at31.25Hz. While Figure 13 show z-axis graphs, the highest amplitude before apply eddy current is 0.7mVolt at frequency 35.16Hz after using eddy current the lowest amplitude drop to 0.35mVolt at 35.16Hz at using 2 poles.

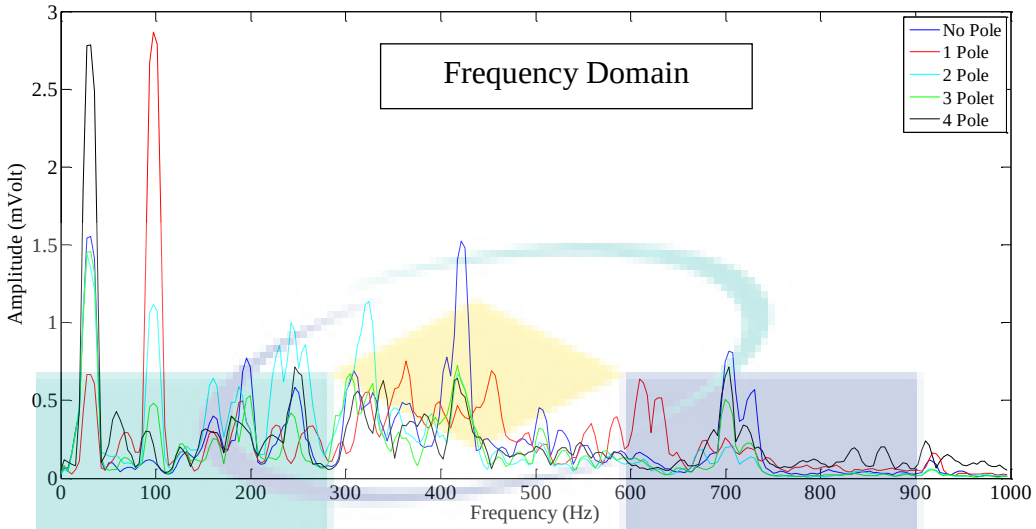

Figure 11. Frequency domain graph for x-axis using 120Volt power supply

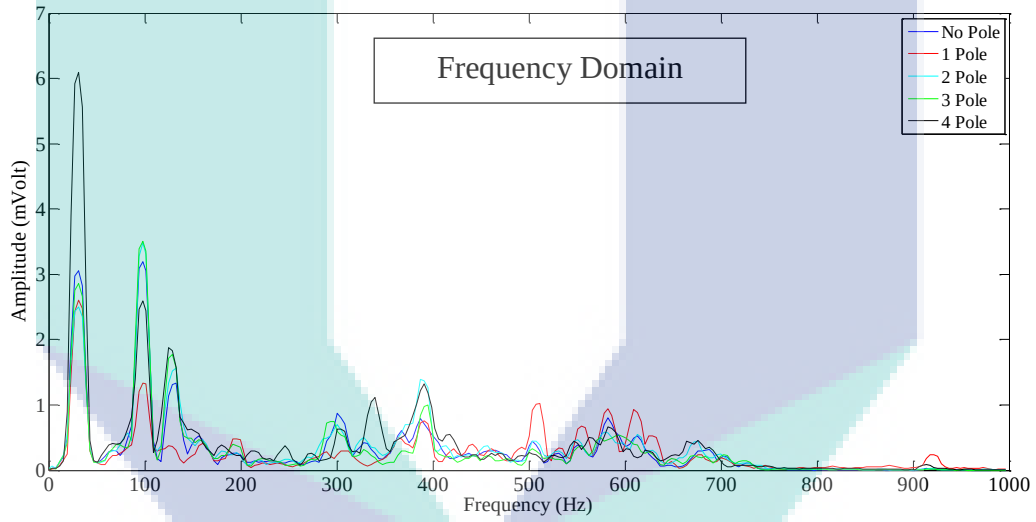

Figure 12. Frequency domain graph for y-axis using 120Volt power supply

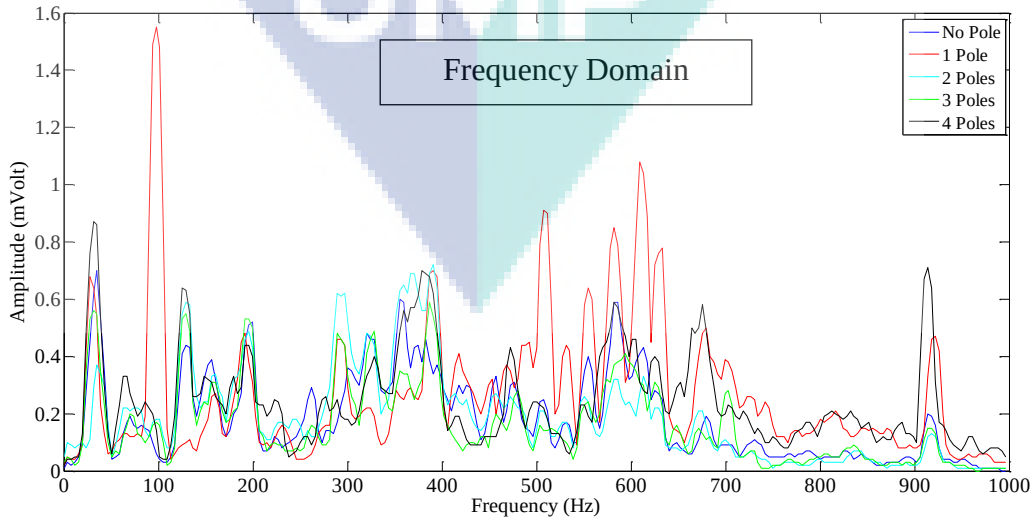

Figure 13. Frequency domain graph for z-axis using 120Volt power supply

Figures 14-16 show the frequency domain graph with 144Volt power supply. From Figure 14 the highest amplitude value before apply eddy current is 1.552mVolt at 31.25 Hz. After apply eddy current, the lowest amplitude is 1.105mVolt at frequency 31.25Hz using 2 eddy current. The second highest amplitude at x-axis is 1.525mVolt at frequency 421.9 Hz, after apply eddy current the lowest amplitude value is 0.2522mVolt at 421.9Hz. Figure 15 representing the y-axis graph with highest amplitude before apply eddy current is 3.19mVolt at 97.66Hz after apply eddy current the lowest amplitude drop is 2.54mVolt at same frequency when using 4 eddy current. Second highest amplitude before apply eddy current is 3.06mVolt at 31.25Hz and suppressed to 2.24mVolt at same frequency. In this graph suppression occurs at frequency in between 300Hz until 500Hz with the amplitude mean of 0.3068mVolt. While Figure 16 show z-axis graphs, the highest amplitude before apply eddy current is 0.7mVolt at frequency 35.16Hz after using eddy current the lowest amplitude drop to 0.29mVolt at 35.16Hz. The amplitude mean for not using eddy current is 0.1836mVolt, 1 eddy current is 0.2731mVolt, 2 eddy current is 0.3248mVolt, 3 eddy current is 0.1299mVolt, 4 eddy current is 0.2812mVolt.

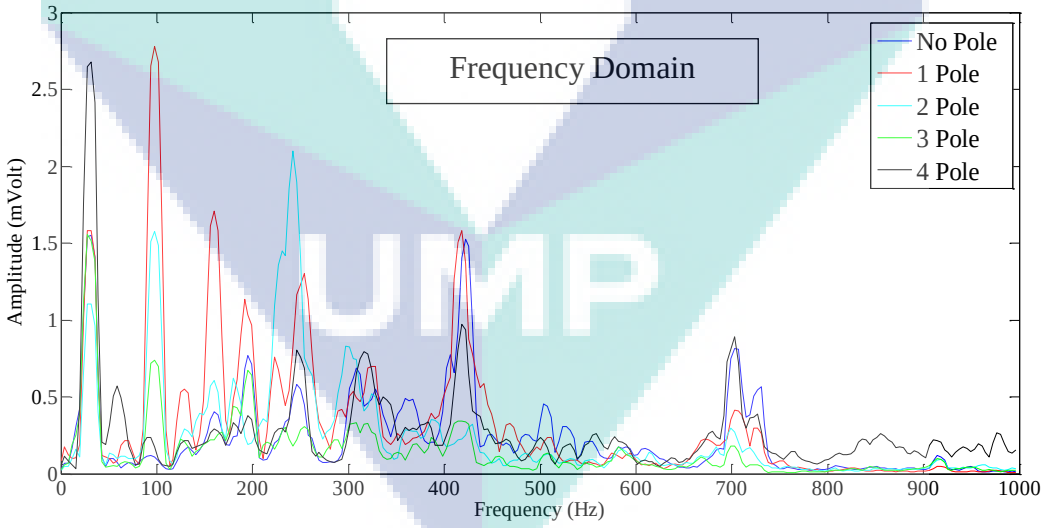

Figure 14. Frequency domain graph for x-axis using 144Volt power supply

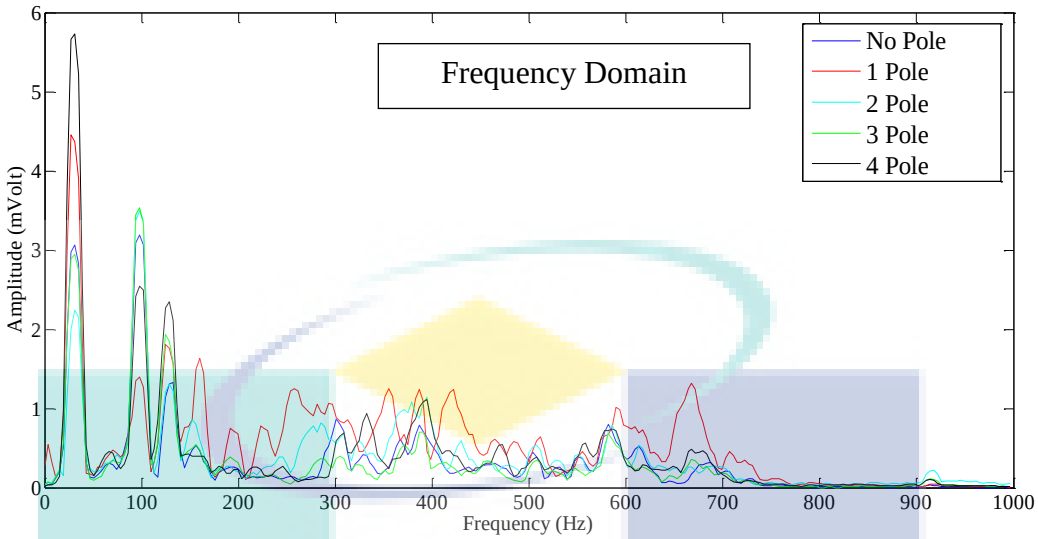

Figure 15. Frequency domain graph for y-axis using 144Volt power supply

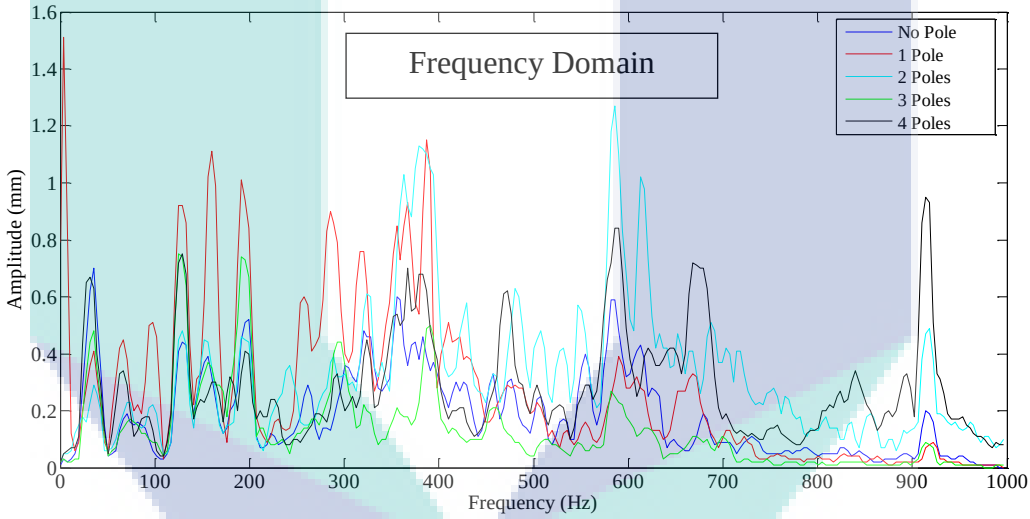

Figure 16. Frequency domain graph for z-axis using 144Volt power supply

2.4.2 Number of Poles at Steering Wheel

Based on Figure 17 it shows that the mean amplitude before apply the pole is 0.2251, mean amplitude for 1 pole is 0.2057, 2 pole is 0.1979, 3 pole is 0.1908 and 4 pole is 0.3311. Related to Figure 18 the mean amplitude before apply the pole is 0.2037, mean amplitude for 1 pole is 0.2079, 2 pole is 0.2108, 3 pole is 0.2164 and 4 pole is 0.3963. While Figure 19 show the mean amplitude before apply the pole is 0.2861, mean amplitude for 1 pole is 0.2731, 2 pole is 0.2965, 3 pole is 0.2904 and 4 pole is 0.3906.

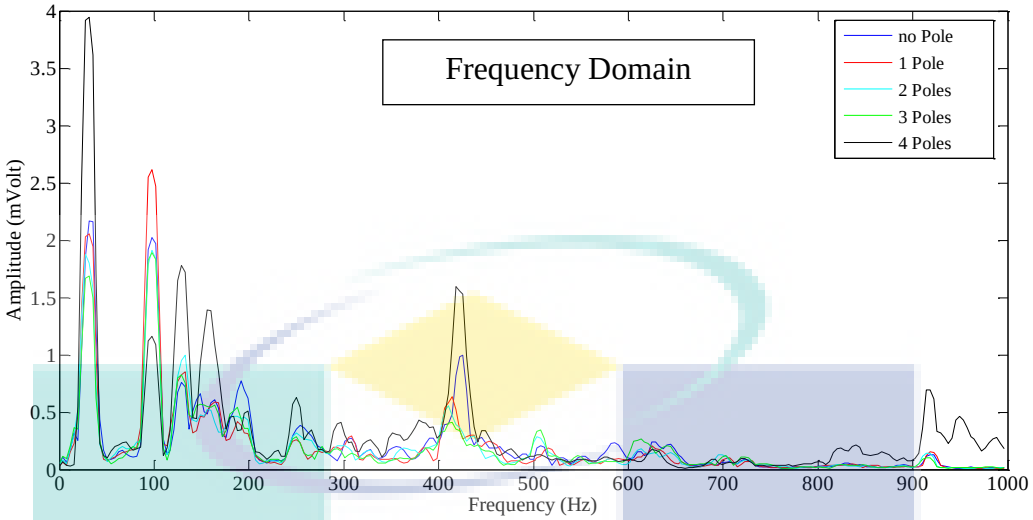

Figure 17. Frequency domain graph for x-axis using 48Volt power supply

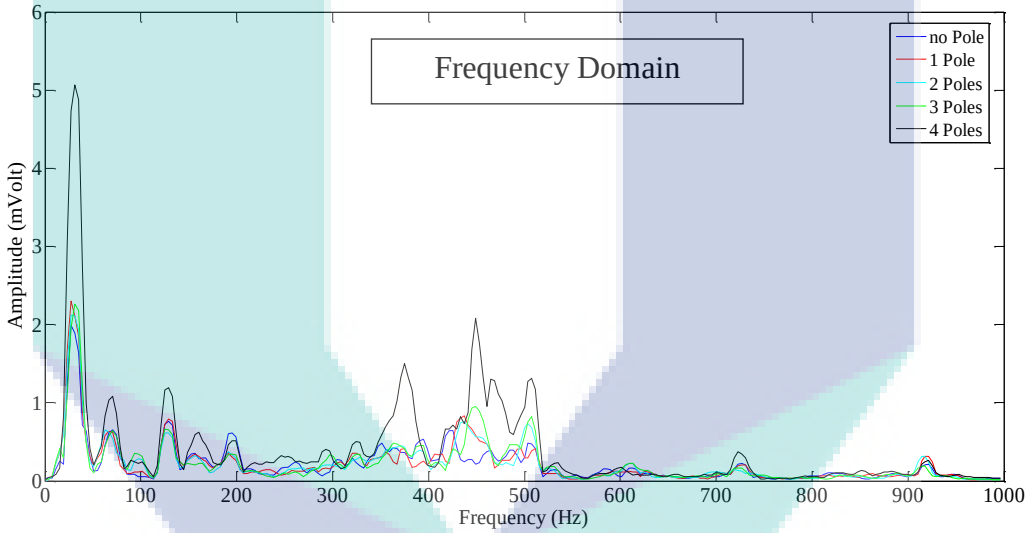

Figure 18. Frequency domain graph for y-axis using 48Volt power supply

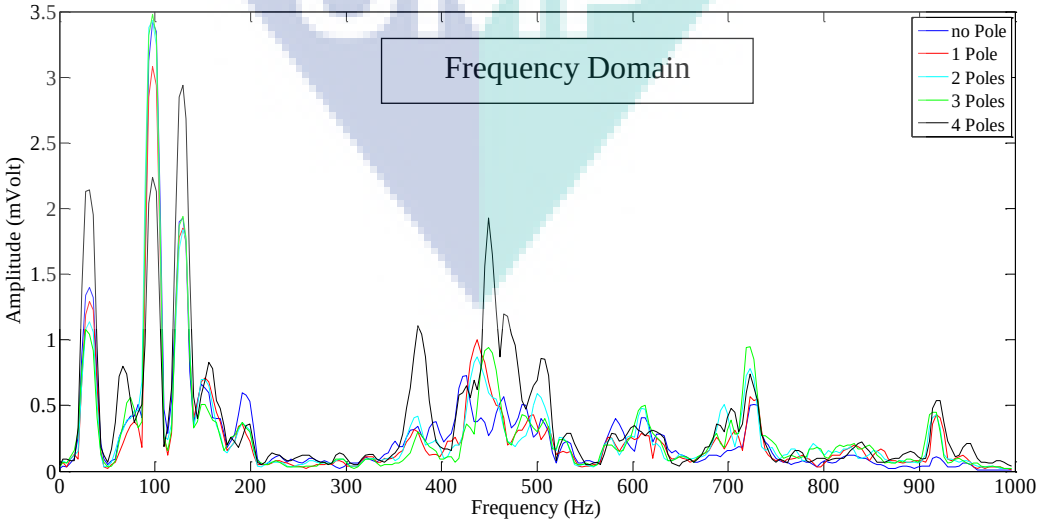

Figure 19. Frequency domain graph for z-axis using 48Volt power supply

At 72volt power supply Figure 20 is shown that the mean amplitude before apply the pole is 0.2251, mean amplitude for 1 pole is 0.2199, 2 pole is 0.1882, 3 pole is 0.1837 and 4 pole is 0.2854. Related to Figure 21 the mean amplitude at y-axis before apply the pole is 0.2037, mean amplitude for 1 pole is 0.1987, 2 pole is 0.2046, 3 pole is 0.203 and 4 pole is 0.3364. While in Figure 22 the mean amplitude before apply the pole is 0.2861, mean amplitude for 1 pole is 0.2544, 2 pole is 0.2825, 3 pole is 0.2787 and 4 pole is 0.3888.

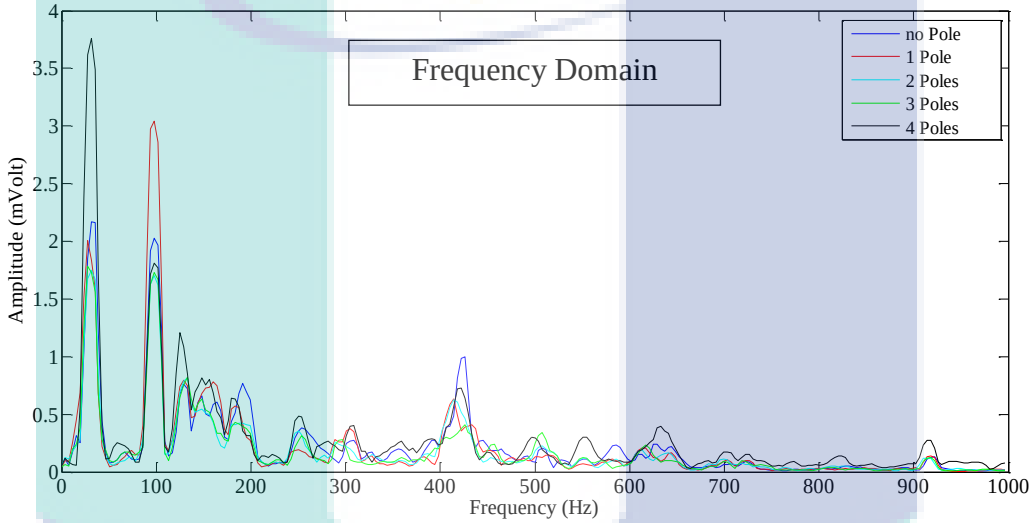

Figure 20. Frequency domain graph for x-axis using 72Volt power supply

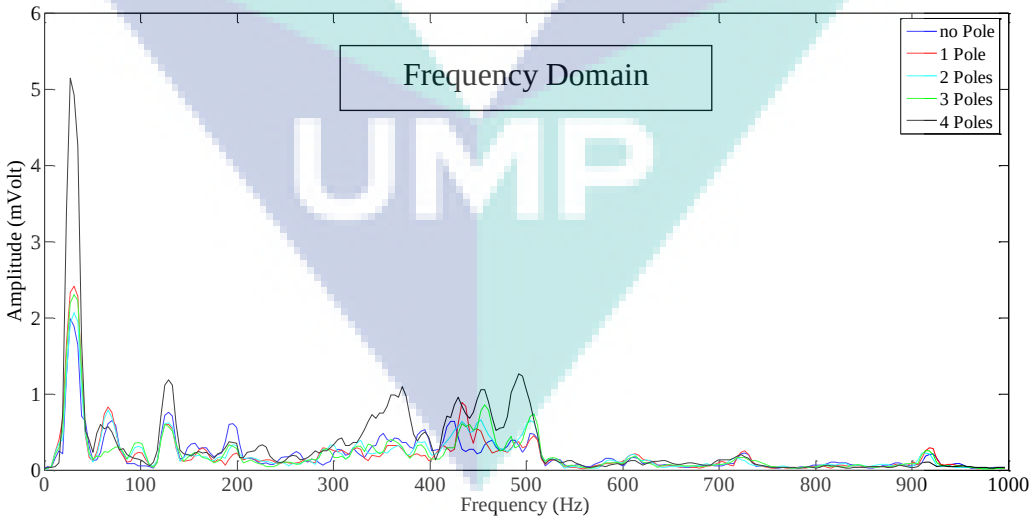

Figure 21. Frequency domain graph for y-axis using 72Volt power supply

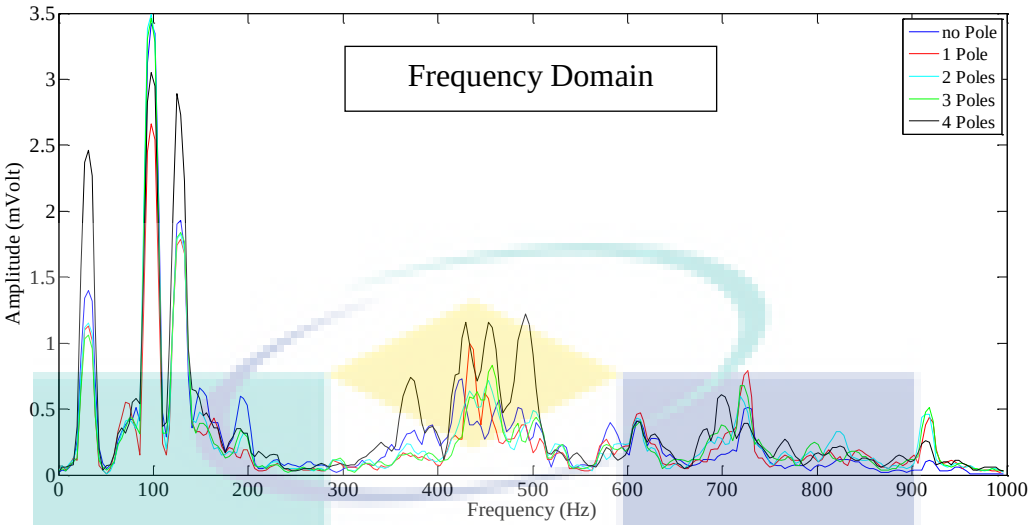

Figure 22. Frequency domain graph for z-axis using 72Volt power supply

While Figure 24 give the mean amplitude before apply the pole is 0.2037, mean amplitude for 1 pole is 0.1964, 2 pole is 0.2125, 3 pole is 0.2101 and 4 pole is 0.3217. Related to Figure 25 the mean amplitude before apply the pole is 0.2861, mean amplitude for 1 pole is 0.2495, 2 pole is 0.2919, 3 pole is 0.2232 and 4 pole is 0.3582. When using 96volt power supply the mean amplitude for Figure 26 before apply the pole is 0.2251, mean amplitude for 1 pole is 0.215, 2 pole is 0.1836, 3 pole is 0.1696 and 4 pole is 0.2931.

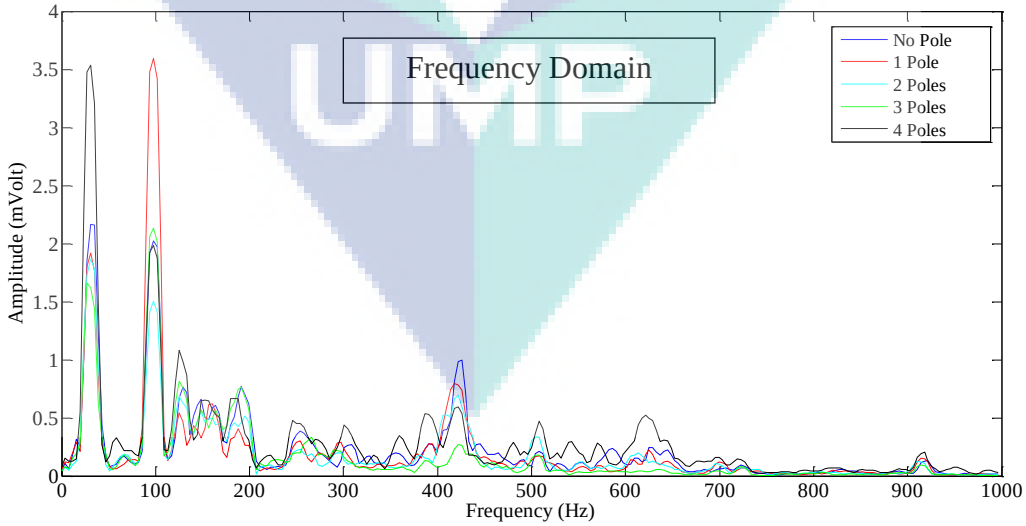

Figure 23. Frequency domain graph for x-axis using 96Volt power supply

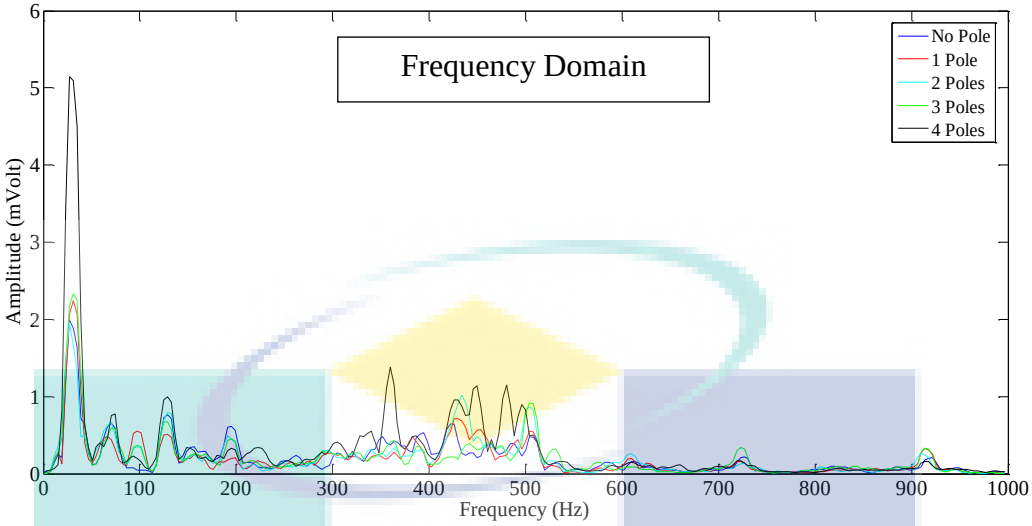

Figure 24. Frequency domain graph for y-axis using 96Volt power supply

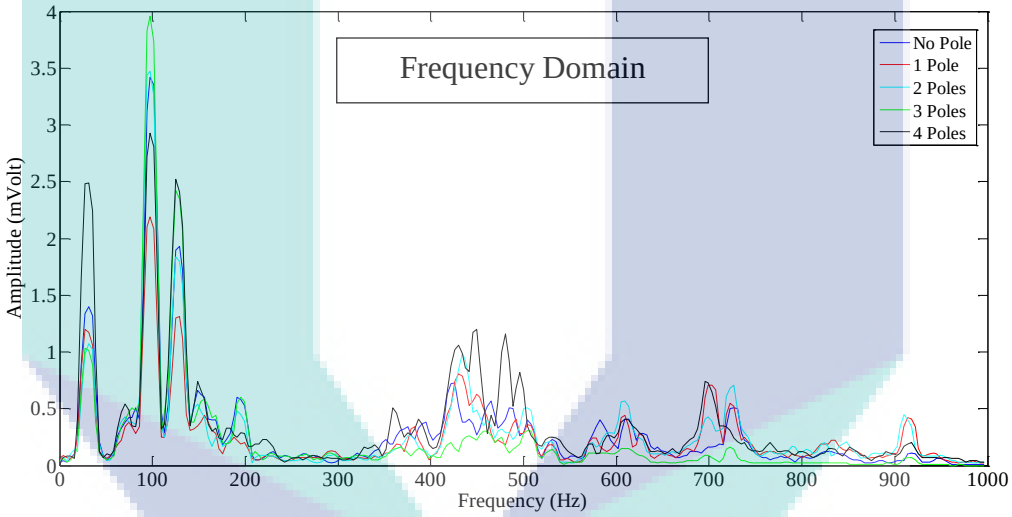

Figure 25. Frequency domain graph for z-axis using 96Volt power supply

At 120volt power supply Figure 26 show the x-axis graph with mean amplitude before apply the pole is 0.2251, mean amplitude for 1 pole is 0.3474, 2 pole is 0.1893, 3 pole is 0.1901 and 4 pole is 0.2893. Related to Figure 27, the mean amplitude before apply the pole is 0.2037, mean amplitude for 1 pole is 0.2547, 2 pole is 0.2253, 3 pole is 0.2161 and 4 pole is 0.338. While in Figure 28 the mean amplitude before apply the pole is 0.2861, mean amplitude for 1 pole is 0.3143, 2 pole is 0.2948, 3 pole is 0.2984 and 4 pole is 0.3452.

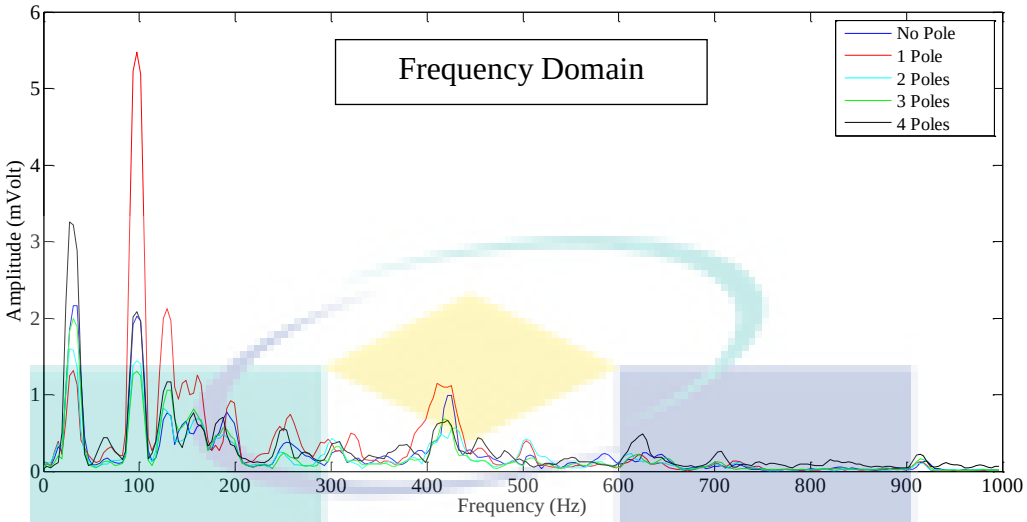

Figure 26. Frequency domain graph for x-axis using 120Volt power supply

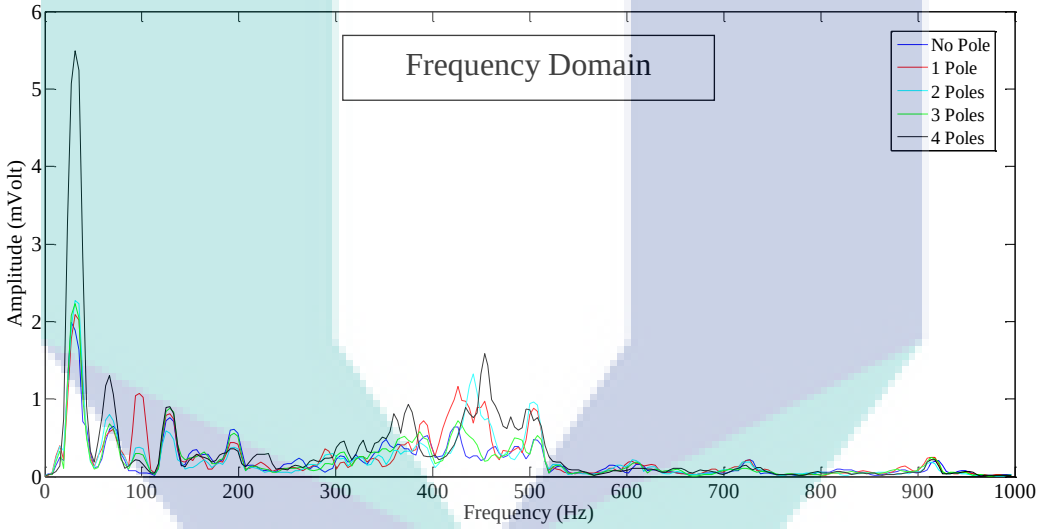

Figure 27. Frequency domain graph for y-axis using 120Volt power supply

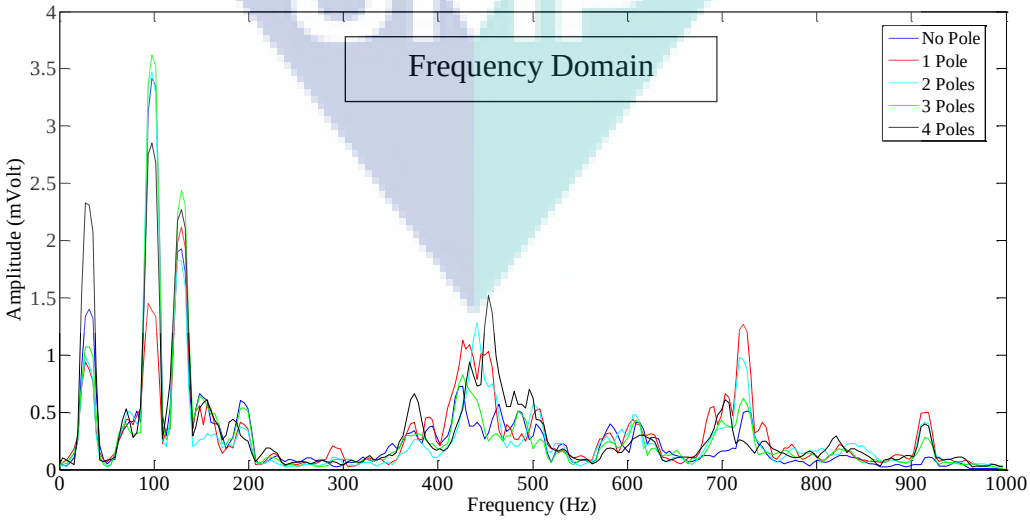

Figure 28. Frequency domain graph for z-axis using 120Volt power supply

When the power supply is increase to 144volt, Figure 29 give the mean amplitude before apply the pole is 0.2251, mean amplitude for 1 pole is 0.4846, 2 pole is 0.2153, 3 pole is 0.197 and 4 pole is 0.2779. While Figure 30 show the mean amplitude before apply the pole is 0.2037, mean amplitude for 1 pole is 0.3317, 2 pole is 0.2221, 3 pole is 0.2082 and 4 pole is 0.3338. Lastly, in Figure 31, the mean amplitude before apply the pole is 0.2861, mean amplitude for 1 pole is 0.3852, 2 pole is 0.2907, 3 pole is 0.2835 and 4 pole is 0.3465.

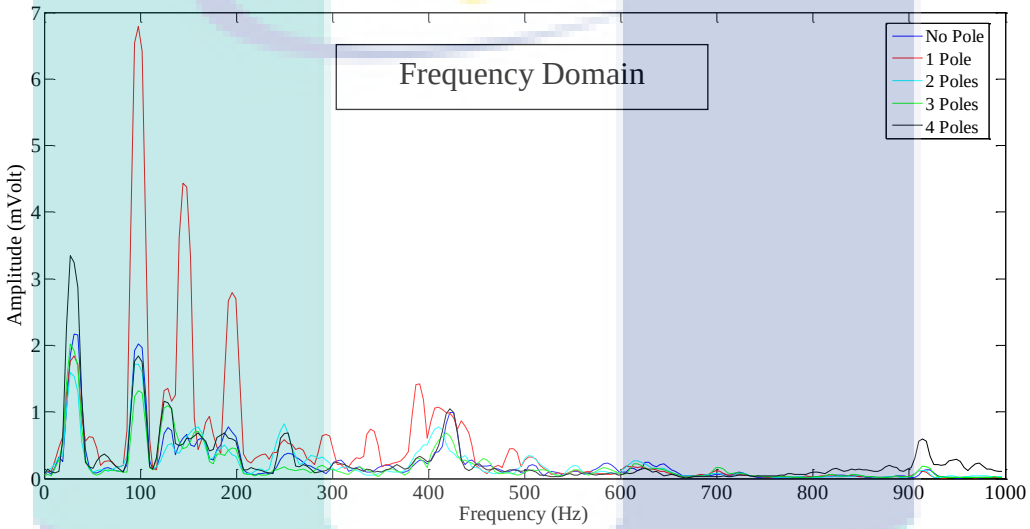

Figure 29. Frequency domain graph for x-axis using 144Volt power supply

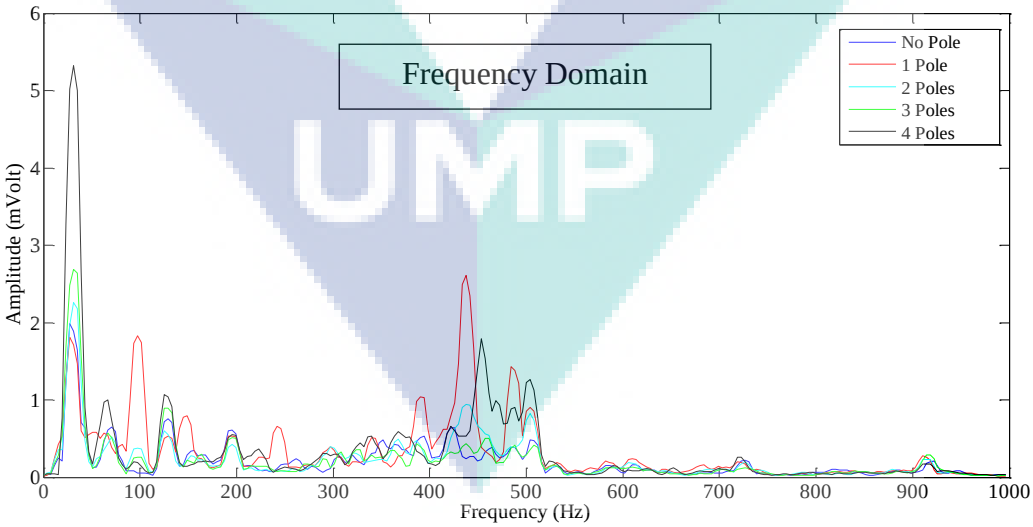

Figure 30. Frequency domain graph for y-axis using 144Volt power supply

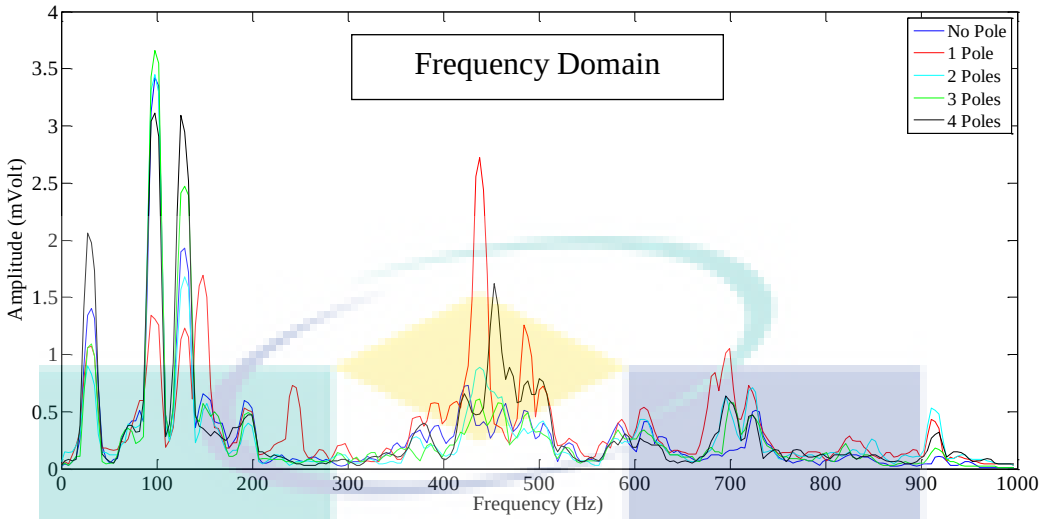

Figure 31. Frequency domain graph for z-axis using 144Volt power supply

2.4.3 Distance of Air Gaps Measure for Aluminium Disc

Figure 32 show frequency domain graph for 2mm air gap at x-axis. Mean amplitude before apply the voltage is 0.2348mVolt, after supply 48Volt the mean amplitude increase to 0.2462mVolt, followed by the 72Volt mean amplitude decrease to 0.2375mVolt. When the voltage increases to 96Volt the mean amplitude again increase to 0.2562mVolt. While with the voltage supply of 120Volt mean of amplitude decrease to 0.2436mVolt and when the voltage supply increase to 144Volt mean amplitude increase to 0.2742mVolt. Minimum mean amplitude after apply voltage is 0.2375mVolt at 72Volt. From the graph, vibration suppression does not occur at x-axis using 2mm air gaps opening. Regarding to formula of eddy current damping force, air gaps is directly proportional with the eddy current damping force. When air gaps decrease, eddy current damping force will increase.

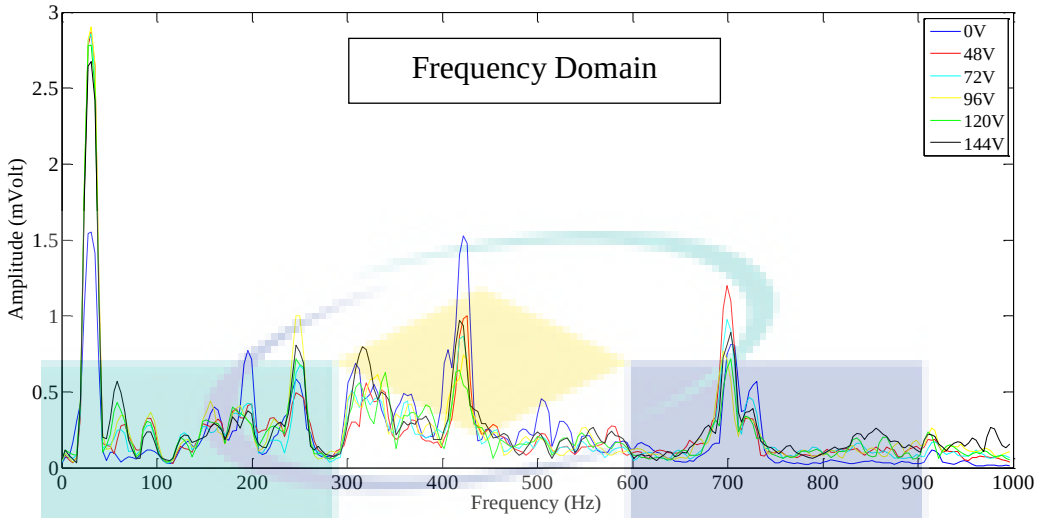

Figure 32. Frequency domain graph for x-axis using 2mm air gaps

Figure 33 show frequency domain graph for 2mm air gap at y-axis. Mean amplitude before apply the voltage is 0.2806mVolt, after supply 48Volt the mean amplitude increase to 0.413mVolt, followed by the 72Volt mean amplitude decrease to 0.4314mVolt. When the voltage increases to 96Volt the mean amplitude again decrease to 0.4176mVolt. While with the voltage supply of 120Volt mean of amplitude decrease to 0.3839mVolt and when the voltage supply increase to 144Volt mean amplitude reduce to 0.3817mVolt. Minimum mean amplitude after apply voltage is 0.3817mVolt at 144Volt. From the graph, vibration suppression does not occur at y-axis using 2mm air gaps opening. Regarding to formula of eddy current damping force, air gaps is directly proportional with the eddy current damping force. When air gaps decrease, eddy current damping force will increase.

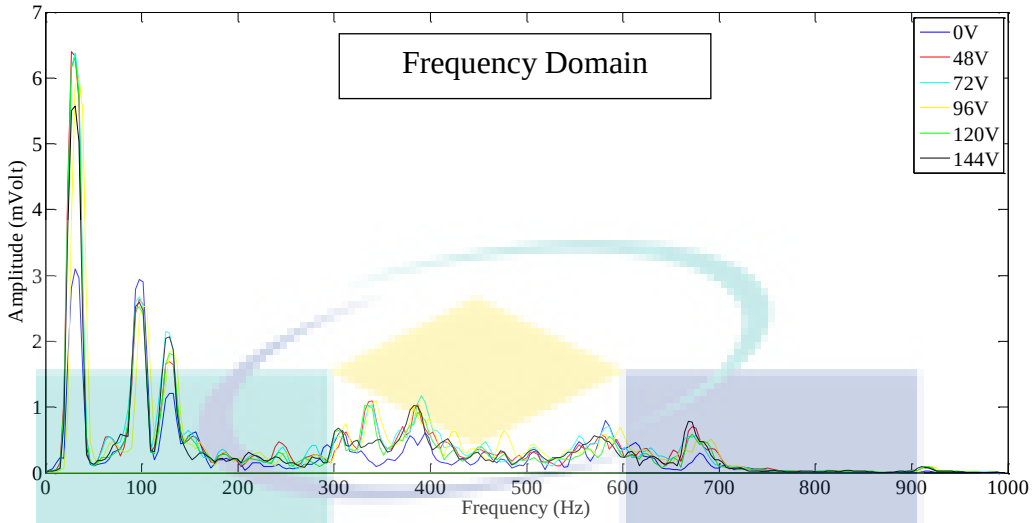

Figure 33. Frequency domain graph for y-axis using 2mm air gaps

Figure 34 show frequency domain graph for 2mm air gap at z-axis. Mean amplitude before apply the voltage is 0.1836mVolt, after supply 48Volt the mean amplitude increase to 0.2438mVolt, followed by the 72Volt mean amplitude increase to 0.2561mVolt. When the voltage increases to 96Volt the mean amplitude again increase to 0.2589mVolt. While with the voltage supply of 120Volt mean of amplitude decrease to 0.2318mVolt and when the voltage supply increase to 144Volt mean amplitude increase to 0.2824mVolt. Minimum mean amplitude after apply voltage is 0.2318mVolt at 120Volt. From the graph, vibration suppression does not occur at z-axis using 2mm air gaps opening because it does not exceed mean amplitude before apply voltage. Regarding to formula of eddy current damping force, air gaps is directly proportional with the eddy current damping force. When air gaps decrease, eddy current damping force will increase.

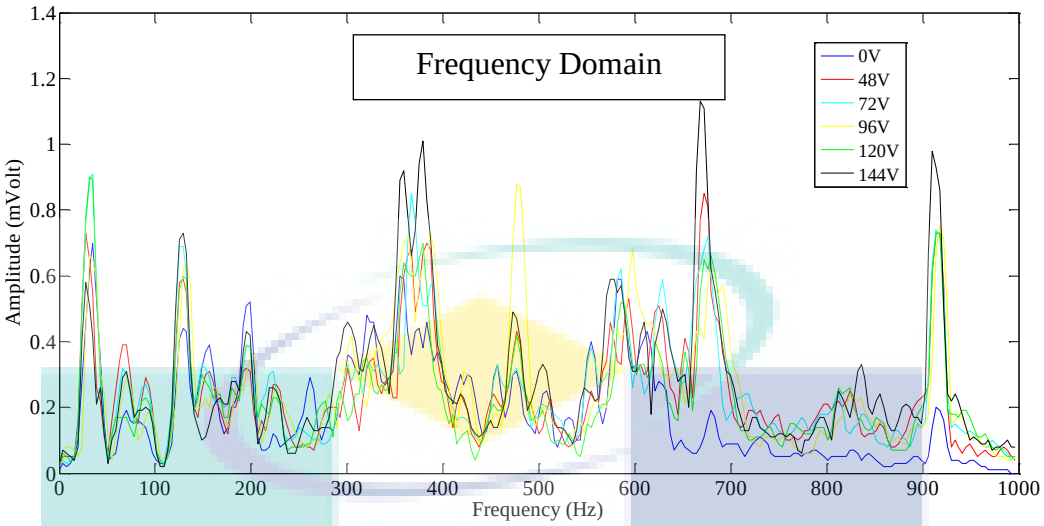

Figure 34. Frequency domain graph for z-axis using 2mm air gaps

Figure 35 show frequency domain graph for 4mm air gap at x-axis. Mean amplitude before apply the voltage is 0.2348mVolt, after supply 48Volt the mean amplitude reduce to 0.2268mVolt, followed by the 72Volt mean amplitude decrease to 0.2168mVolt. When the voltage increases to 96Volt the mean amplitude again decrease to 0.2153mVolt. While with the voltage supply of 120Volt mean of amplitude decrease to 0.2117mVolt and when the voltage supply increase to 144Volt mean amplitude increase to 0.2243mVolt. Minimum mean amplitude after apply voltage is 0.2117mVolt at 120Volt. From the theory of eddy current damping force, current is directly proportional to eddy current damping force. When current induce increase, eddy current damping force is also increase. From the graph it shows that highest vibration suppression at 120volt power supply.

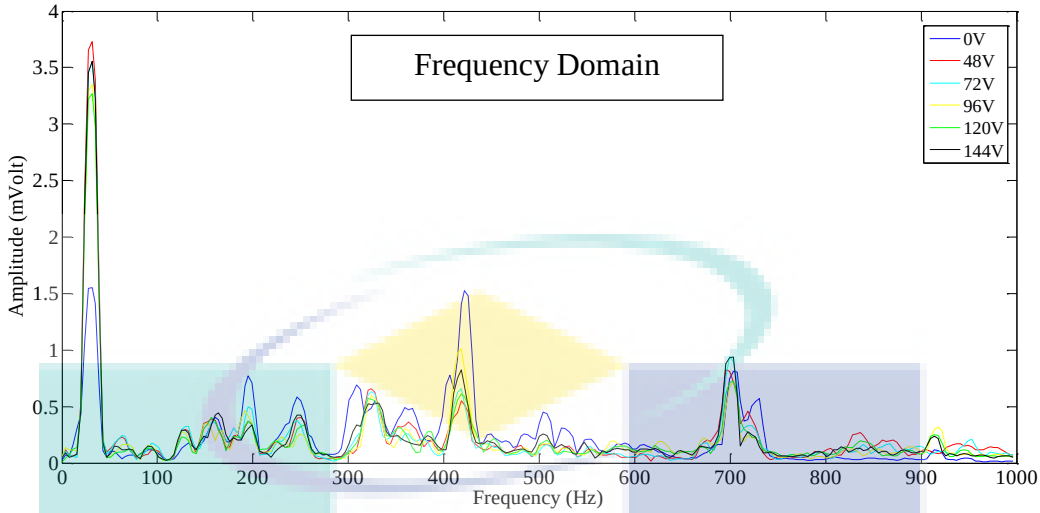

Figure 35. Frequency domain graph for x-axis using 4mm air gaps

Figure 36 show frequency domain graph for 4mm air gap at y-axis. Mean amplitude before apply the voltage is 0.3139mVolt, after supply 48Volt the mean amplitude increase to 0.3684mVolt, followed by the 72Volt mean amplitude decrease back to 0.3543mVolt. When the voltage increases to 96Volt the mean amplitude again decrease to 0.3505mVolt. While with the voltage supply of 120Volt mean of amplitude decrease to 0.3419mVolt and when the voltage supply increase to 144Volt mean amplitude increase to 0.3495mVolt. Minimum mean amplitude after apply voltage is 0.3419mVolt at 120Volt. From the theory of eddy current damping force, current is directly proportional to eddy current damping force. When current induce increase, eddy current damping force is also increase. From the graph it shows that highest vibration suppression at 120volt power supply.

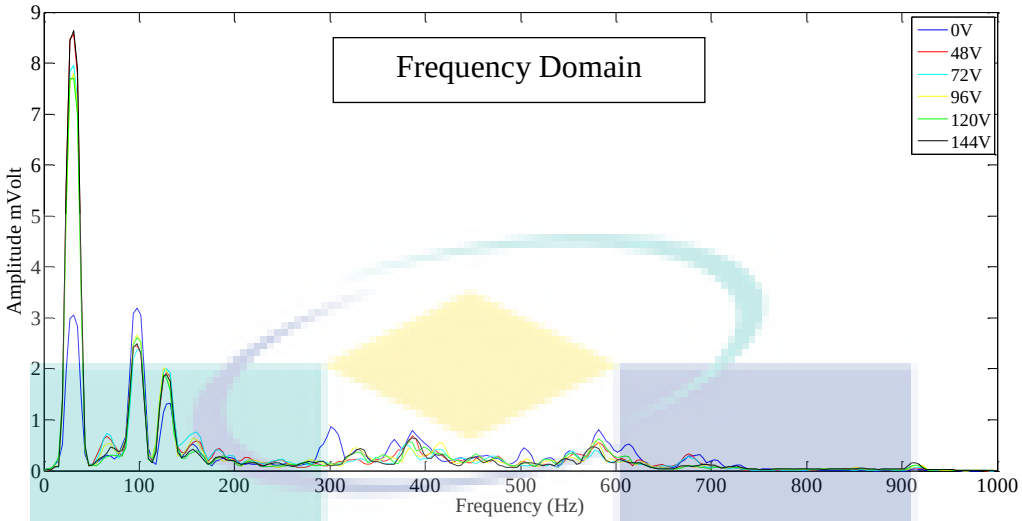

Figure 36. Frequency domain graph for y-axis using 4mm air gaps

Figure 37 show frequency domain graph for 4mm air gap at z-axis. Mean amplitude before apply the voltage is 0.1933mVolt, after supply 48Volt the mean amplitude increase to 0.2321mVolt, followed by the 72Volt mean amplitude decrease back to 0.2239mVolt. When the voltage increases to 96Volt the mean amplitude again decrease to 0.2055mVolt. While with the voltage supply of 120Volt mean of amplitude decrease to 0.2073mVolt and when the voltage supply increase to 144Volt mean amplitude increase to 0.2122mVolt. Minimum mean amplitude after apply voltage is 0.2055mVolt at 96Volt. From the theory of eddy current damping force, current is directly proportional to eddy current damping force. When current induce increase, eddy current damping force is also increase. From the graph it shows that highest vibration suppression at 120volt power supply.

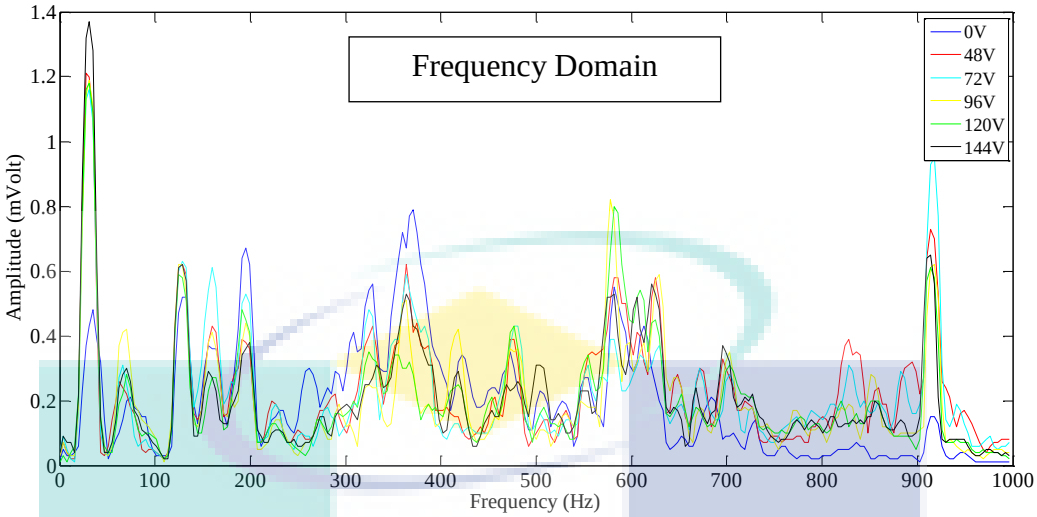

Figure 37. Frequency domain graph for z-axis using 4mm air gaps

Figure 38 show frequency domain graph for 6mm air gap at x-axis. Mean amplitude before apply the voltage is 0.2348mVolt, after supply 48Volt the mean amplitude reduce to 0.2235mVolt followed by the 72Volt mean amplitude reduce to 0.2112mVolt. When the voltage increase to 96Volt the mean amplitude again reduce to 0.2016mVolt. But mean of amplitude will increase when the voltage supply at 120Volt and 144Volt which are 0.2815mVolt and 0.2855mvolt. In this graph the minimum mean amplitude is 0.2016mVolt at 96Volt.

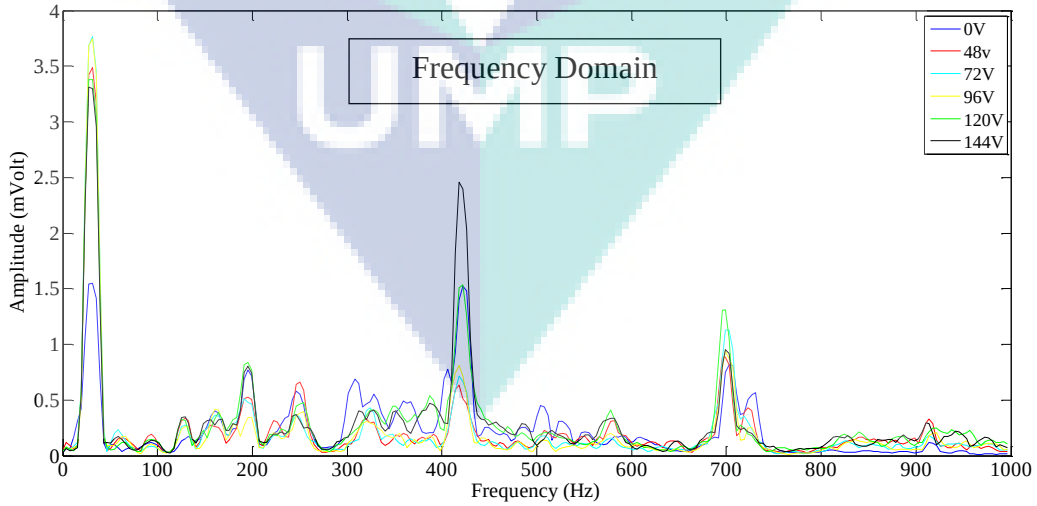

Figure 38. Frequency domain graph for x-axis using 6mm air gaps

Figure 39 show frequency domain graph for 6mm air gap at y-axis. Mean amplitude before apply the voltage is 0.3139mVolt, after supply 48Volt the mean amplitude increase to 0.3364mVolt, followed by the 72Volt mean amplitude increase to 0.3465mVolt. When the voltage increase to 96Volt the mean amplitude again increase to 0.3574mVolt. The mean of amplitude will increase when the voltage supply at 120Volt and 144Volt which are 0.4583mVolt and 0.4535mvolt. Minimum mean amplitude after apply eddy current is 0.3364mVolt at 48Volt.

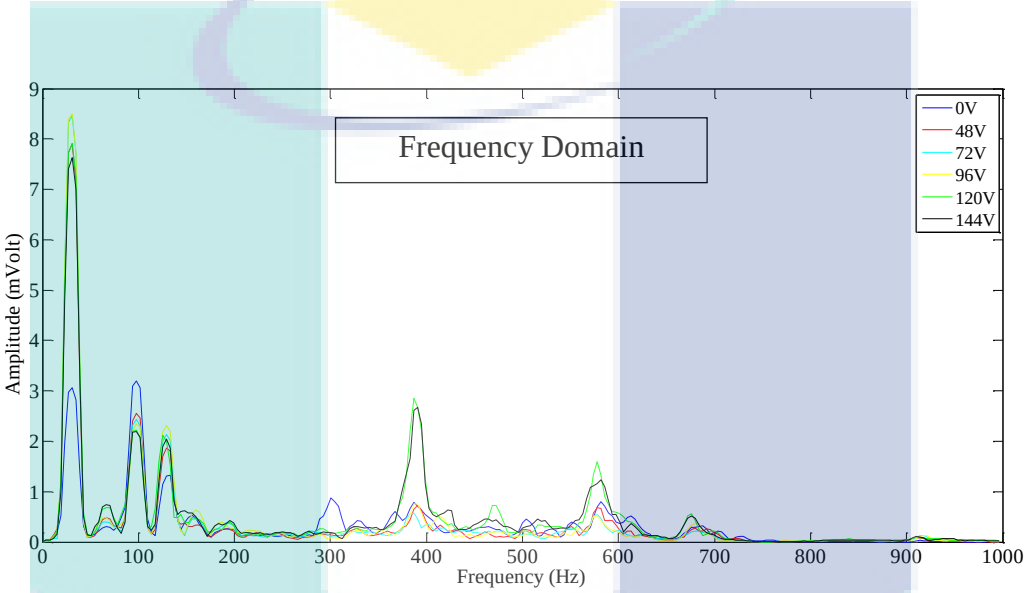

Figure 39. Frequency domain graph for y-axis using 6mm air gaps

Figure 40 show frequency domain graph for 6mm air gap at z-axis. Mean amplitude before apply the voltage is 0.1933mVolt, after supply 48Volt the mean amplitude increase to 0.2059mVolt, followed by the 72Volt mean amplitude decrease to 0.1979mVolt. When the voltage increase to 96Volt the mean amplitude again increases to 0.1981mVolt. The mean of amplitude will increase when the voltage supplies at 120Volt and 144Volt which are 0.3339mVolt and 0.3145mvolt. The minimum mean amplitude after apply eddy current is 0.1979mVolt at 96Volt. But it still does not suppress the vibration because of the increase in air gap value.

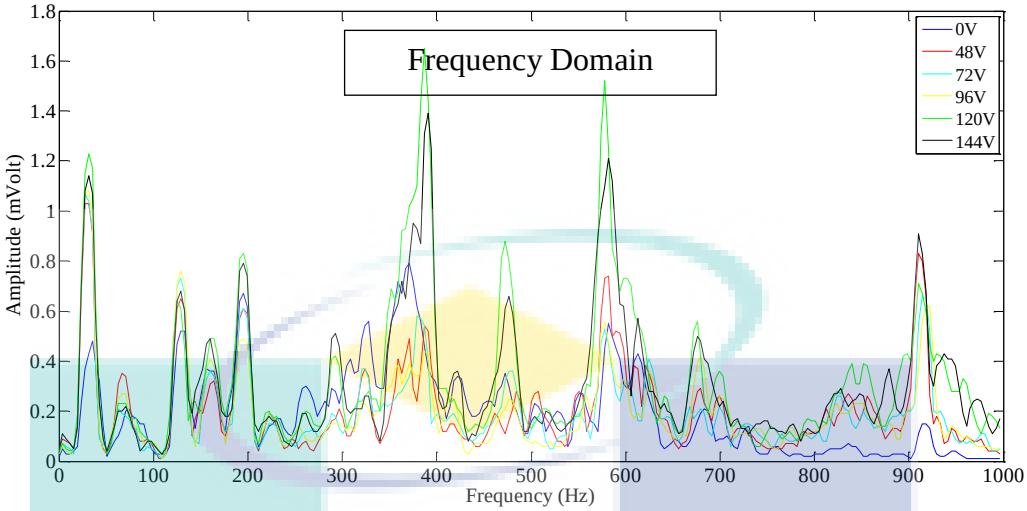

Figure 40. Frequency domain graph for z-axis using 6mm air gaps

2.4.4 Distance of Air Gaps Measure for Steering Wheel

Figure 41 show frequency domain graph for 2mm air gap at x-axis. Mean amplitude before apply the voltage is 0.2251mVolt, after supply 48Volt the mean amplitude increase to 0.3311mVolt followed by the 72Volt mean amplitude reduce to 0.2854mVolt. When the voltages increase to 96Volt the mean amplitude again increase to 0.2931mVolt. While when the voltage increase to 120Volt mean amplitude is 0.2893mVolt and 144Volt mean amplitude decrease to 0.2779mVolt. In this graph the minimum mean amplitude after apply voltage is 0.2779mVolt at 144Volt. The vibration suppression does not occur at x-axis because the mean amplitude after apply voltage is higher than the mean amplitude before apply voltage.

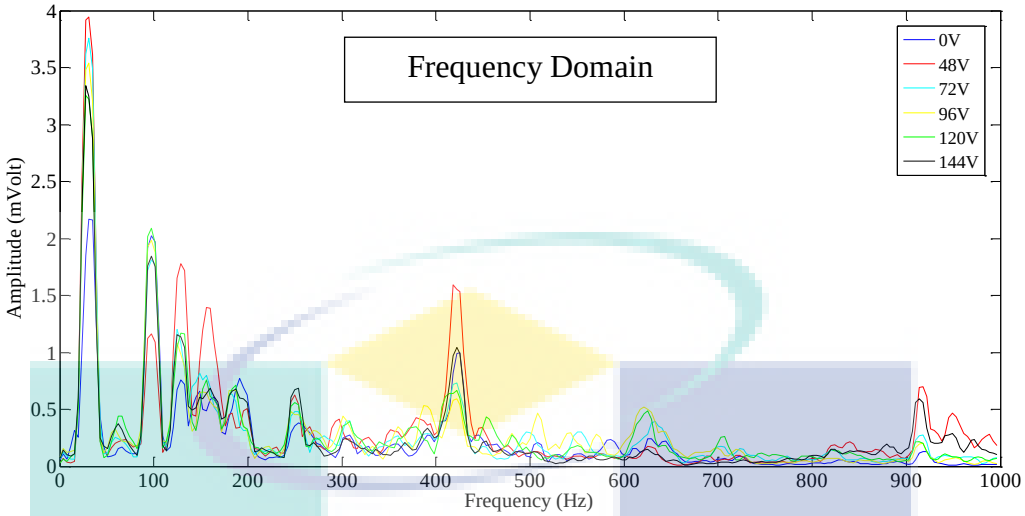

Figure 41. Frequency domain graph for x-axis using 2mm air gaps

Figure 42 show frequency domain graph for 2mm air gap at y-axis. Mean amplitude before apply the voltage is 0.2037mVolt, after supply 48Volt the mean amplitude increase to 0.3963mVolt, followed by the 72Volt mean amplitude decrease to 0.3364mVolt. When the voltage increases to 96Volt the mean amplitude again decrease to 0.3217mVolt. While with the voltage supply of 120Volt mean of amplitude is 0.338mVolt and when the voltage supply increase to 144Volt mean amplitude is 0.3338mvolt. Minimum mean amplitude after apply voltage is 0.3217mVolt at 96Volt. The vibration suppression does not occur at y-axis because the mean amplitude after apply voltage is higher than mean amplitude before apply voltage.

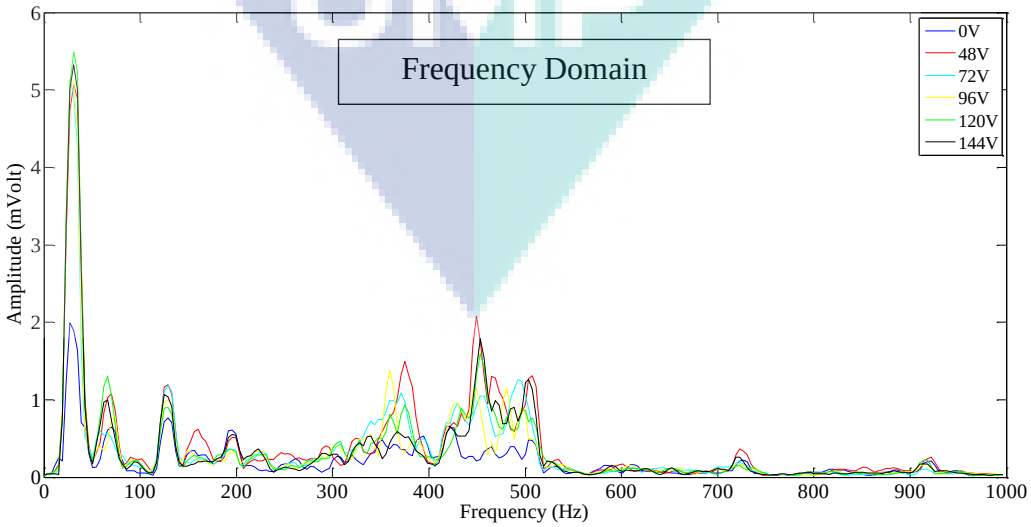

Figure 42. Frequency domain graph for y-axis using 2mm air gaps

Figure 43 show frequency domain graph for 2mm air gap at z-axis. Mean amplitude before apply the voltage is 0.2861mVolt, after supply 48Volt the mean amplitude increase to 0.3906mVolt, followed by the 72Volt mean amplitude increase to 0.3888mVolt. When the voltage supplies of 96Volt the mean amplitude decrease to 0.3582mVolt. While with the voltage supply of 120Volt mean of amplitude decrease to 0.3452mVolt and when the voltage supply increase to 144Volt mean amplitude increase to 0.3465mVolt. Minimum mean amplitude after apply voltage is 0.3452mVolt at 120Volt. The vibration suppression does not occur at z-axis because the mean amplitude at 120Volt is higher than mean amplitude before apply the voltage.

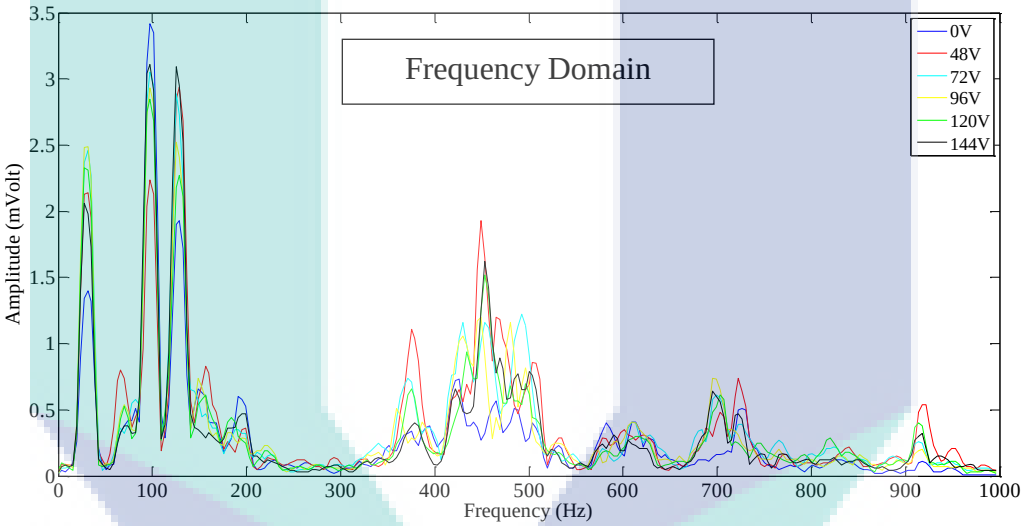

Figure 43. Frequency domain graph for z-axis using 2mm air gaps

Figure 44 show frequency domain graph for 4mm air gap at x-axis. Mean amplitude before apply the voltage is 0.2251mVolt, after supply 48Volt the mean amplitude increase to 0.39mVolt, followed by the 72Volt mean amplitude decrease to 0.2601mVolt. When the voltage increases to 96Volt the mean amplitude again increase to 0.2659mVolt. While with the voltage supply of 120Volt mean of amplitude decrease to 0.2522mVolt and when the voltage supply is 144Volt mean amplitude increase to 0.2678mVolt. Minimum mean amplitude after apply voltage is 0.2522mVolt at 120Volt. The vibration suppression does not occur at x-axis. This is because the mean amplitude value at 120Volt is higher than mean amplitude before apply the voltage.

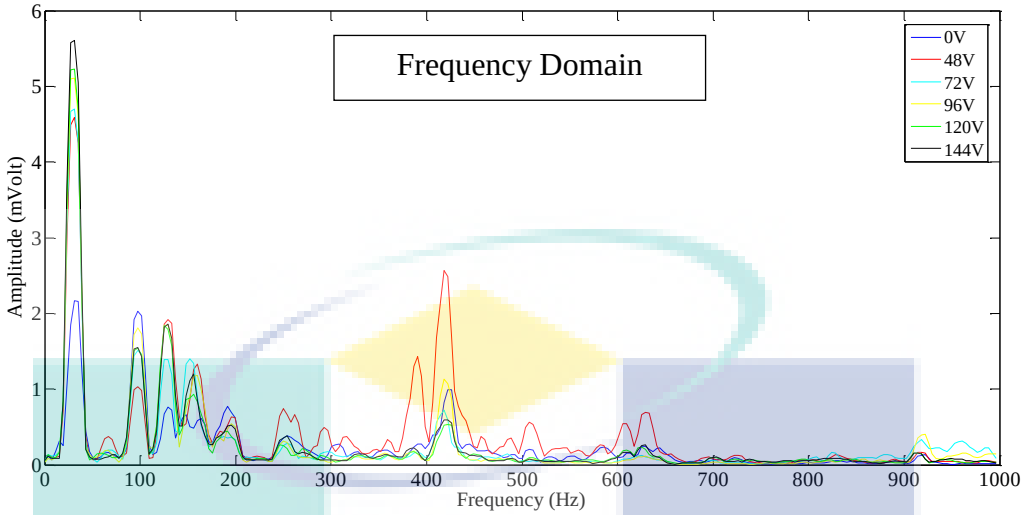

Figure 44. Frequency domain graph for x-axis using 4mm air gaps

Figure 45 show frequency domain graph for 4mm air gap at y-axis. Mean amplitude before apply the voltage is 0.2037mVolt, after supply 48Volt the mean amplitude increase to 0.4129mVolt, followed by the 72Volt mean amplitude decrease to 0.313mVolt. When the voltage increases to 96Volt the mean amplitude again decrease to 0.2979mVolt. While with the voltage supply of 120Volt mean of amplitude decrease to 0.288mVolt and when the voltage supply increase to 144Volt mean amplitude increase to 0.2944mVolt. Minimum mean amplitude after apply voltage is 0.288mVolt at 120Volt. The vibration suppression does not occur at x-axis. Because the mean amplitude value at 120Volt is higher than mean amplitude before apply the voltage.

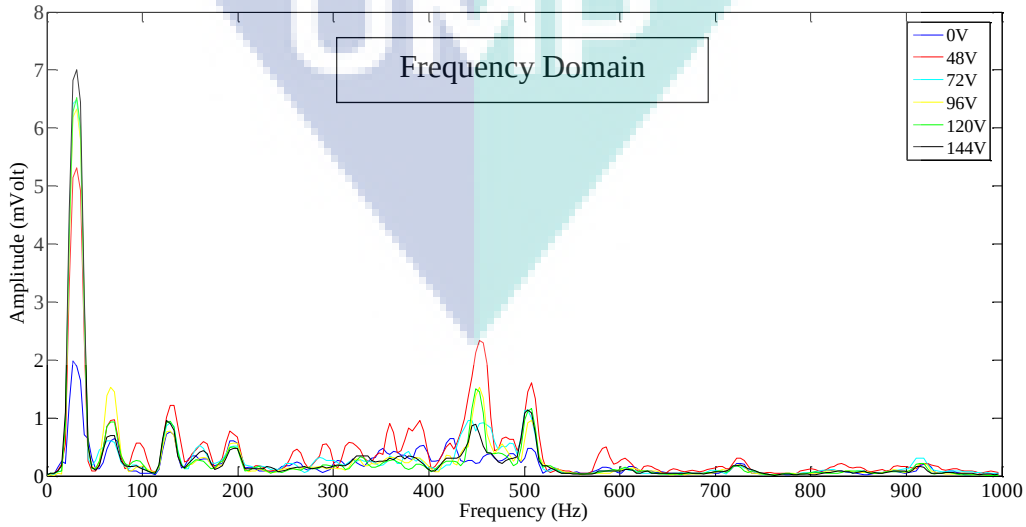

Figure 45. Frequency domain graph for y-axis using 4mm air gaps

Figure 46 show frequency domain graph for 4mm air gap at z-axis. Mean amplitude before apply the voltage is 0.2861mVolt, after supply 48Volt the mean amplitude increase to 0.4364mVolt, followed by the 72Volt mean amplitude decrease to 0.3255mVolt. When the voltage increases to 96Volt the mean amplitude again decrease to 0.3058mVolt. While with the voltage supply of 120Volt mean of amplitude decrease to 0.311mVolt and when the voltage supply increase to 144Volt mean amplitude increase to 0.3156mVolt. Minimum mean amplitude after apply voltage is 0.3058mVolt at 96Volt. The vibration suppression does not occur at x-axis because the mean amplitude value at 96Volt is higher than mean amplitude before apply the voltage.

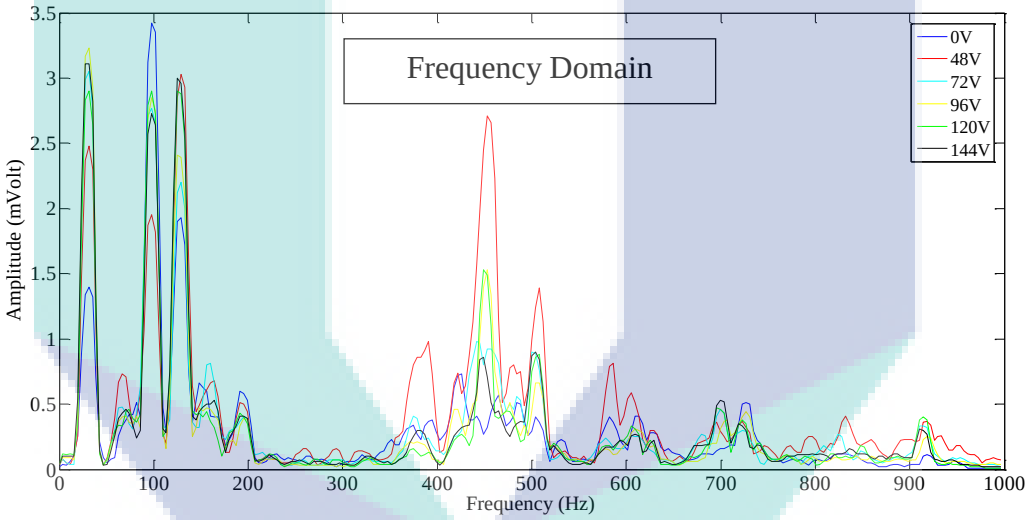

Figure 46. Frequency domain graph for z-axis using 4mm air gaps

Figure 47 show frequency domain graph for 6mm air gap at x-axis. Mean amplitude before apply the voltage is 0.2157mVolt, after supply 48Volt the mean amplitude increase to 0.2698mVolt, followed by the 72Volt mean amplitude decrease to 0.2992mVolt. When the voltage increases to 96Volt the mean amplitude again decrease to 0.2865mVolt. While with the voltage supply of 120Volt mean of amplitude decrease to 0.2833mVolt and when the voltage supply increase to 144Volt mean amplitude increase to 0.337mVolt. Minimum mean amplitude after apply voltage is 0.2698mVolt at 48Volt. The vibration suppression does not occur at x-axis because the mean amplitude value at 48Volt is higher than mean amplitude before apply the voltage.

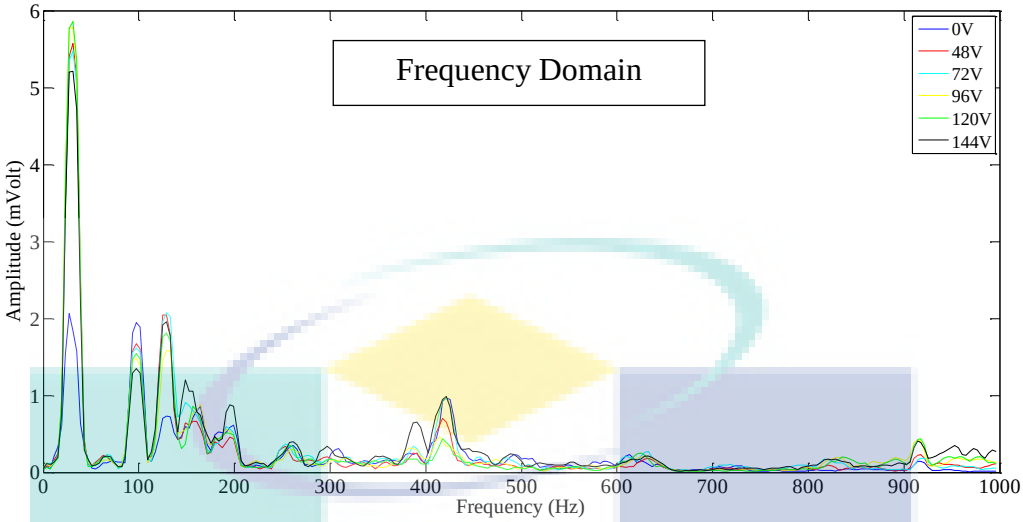

Figure 47. Frequency domain graph for x-axis using 6mm air gaps

Figure 48 show frequency domain graph for 6mm air gap at y-axis. Mean amplitude before apply the voltage is 0.216mVolt, after supply 48Volt the mean amplitude increase to 0.3055mVolt, followed by the 72Volt mean amplitude increase to 0.327mVolt. When the voltage increases to 96Volt the mean amplitude again increase to 0.3503mVolt. While with the voltage supply of 120Volt mean of amplitude increase to 0.3459mVolt and when the voltage supply increase to 144Volt mean amplitude increase to 0.4086mVolt. Minimum mean amplitude after apply voltage is 0.3055mVolt at 48Volt. The vibration suppression does not occur at x-axis because the mean amplitude value at 48Volt is higher than mean amplitude before apply the voltage.

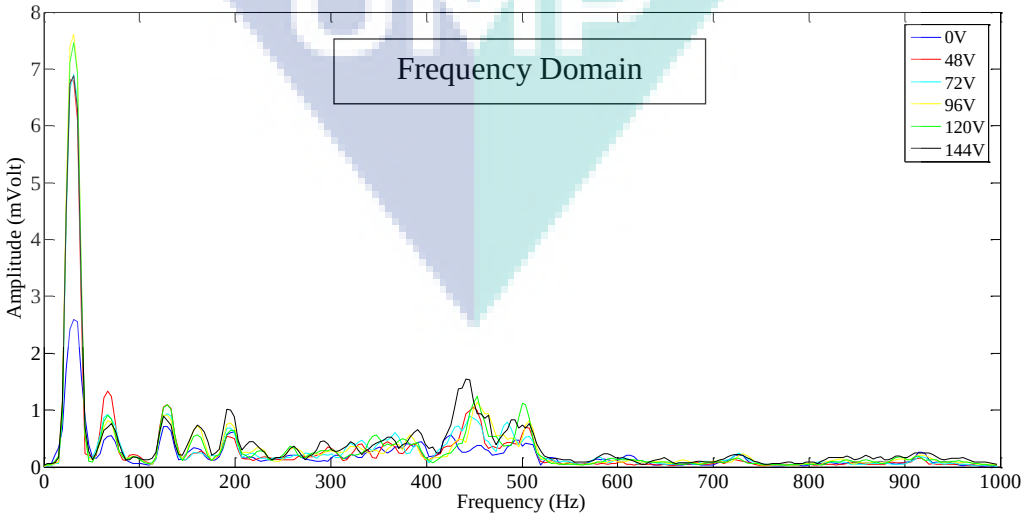

Figure 48. Frequency domain graph for y-axis using 6mm air gaps

Figure 49 show frequency domain graph for 6mm air gap at z-axis. Mean amplitude before apply the voltage is 0.2718mVolt, after supply 48Volt the mean amplitude increase to 0.309mVolt, followed by the 72Volt mean amplitude increase to 0.3464mVolt. When the voltage increases to 96Volt the mean amplitude again increase to 0.3522mVolt. While with the voltage supply of 120Volt mean of amplitude decrease to 0.3508mVolt and when the voltage supply increase to 144Volt mean amplitude increase to 0.4173mVolt. Minimum mean amplitude after apply voltage is 0.309mVolt at 48Volt. The vibration suppression does not occur at x-axis because the mean amplitude value at 48Volt is higher than mean amplitude before apply the voltage.

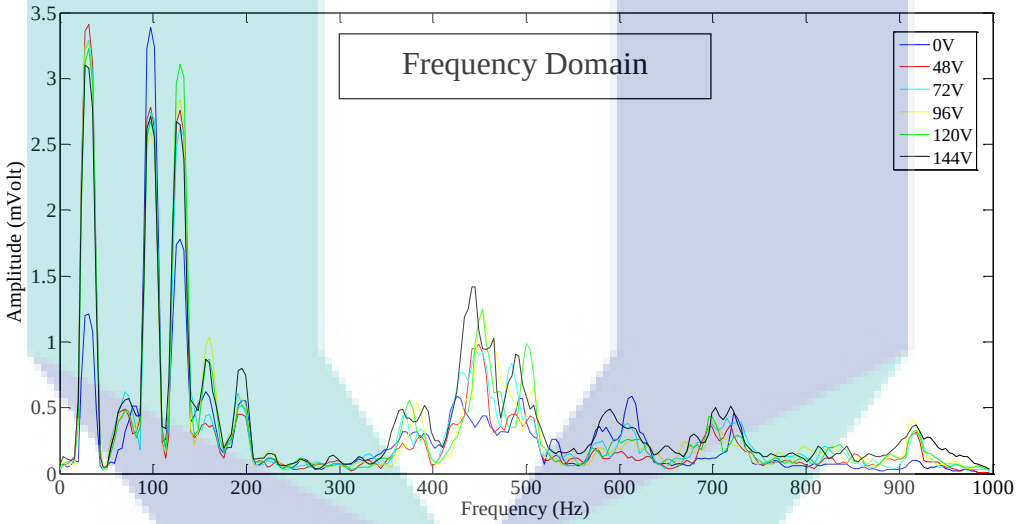

Figure 49. Frequency domain graph for z-axis using 6mm air gaps

2.4.5 Comparison with Different Number of Air Gap

Figures 50-51 shows the frequency domain graph using 2 poles eddy current with accelerometer located at aluminium disc. While Figures 52-53 shows the frequency domain graph using 2 poles eddy current with accelerometer located at steering wheel. The blue colour representing for 2mm air gap, red colour is 4mm air gaps and black colour representing for 6mm air gaps.

Figure 50 above is the x-axis graph acceleration amplitude versus frequency with the different of air gaps opening. The lowest mean amplitude is 0.166mVolt when

air gaps opening is 2mm, mean amplitude for 4mm air gap is 0.2408mVolt while mean amplitude for 6mm air gap is 0.2481mVolt. Figure 4.50 above show the y-axis graph acceleration amplitude versus frequency. The lowest mean amplitude is 0.2787mVolt when air gaps opening is 2mm, mean amplitude for 4mm air gap is 0.3595mVolt while mean amplitude for 6mm air gap is 0.3981mVolt.

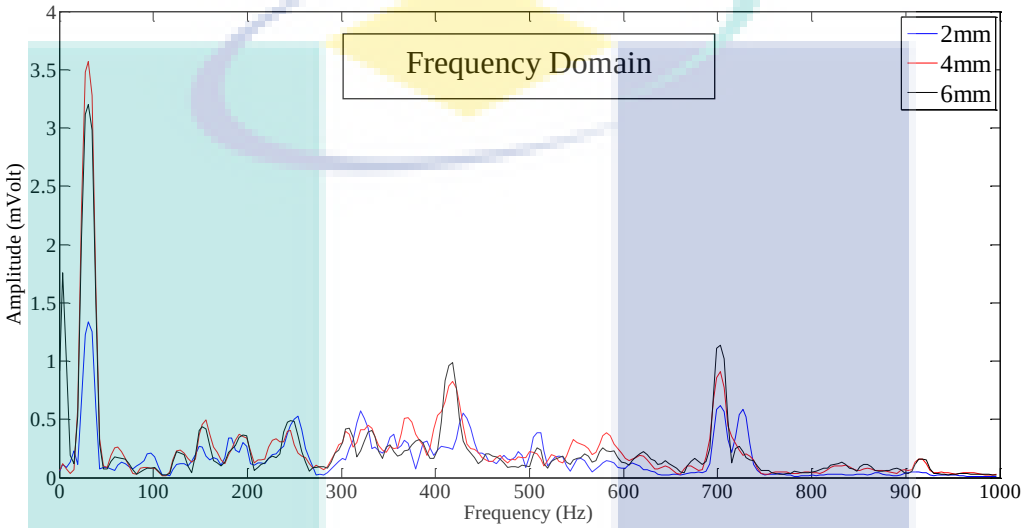

Figure 50. Frequency domain graph for x-axis using 2 poles transformer.

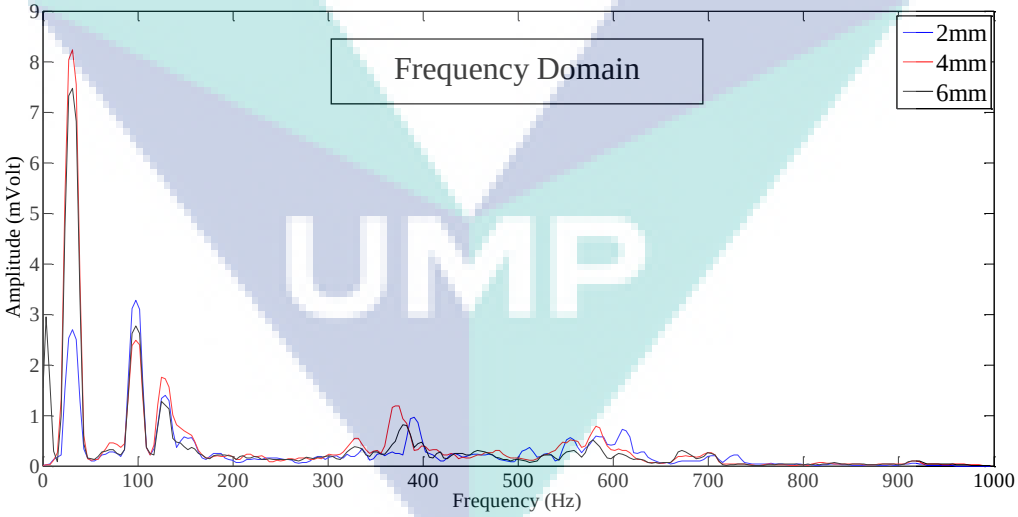

Figure 51. Frequency domain graph for y-axis using 2 poles transformer.

Figure 52 is the x-axis graph acceleration amplitude versus frequency with the different of air gaps opening. The lowest mean amplitude is 0.1979mVolt when air gaps opening 2mm, mean amplitude increase to 0.2456mVolt when suing 4mm air gap while

mean amplitude is higher compare to other with 0.2915mVolt for 6mm air gap. Figure 53 show the y-axis graph acceleration amplitude versus frequency. The lowest mean amplitude is 0.2108mVolt when air gaps opening is 2mm, mean amplitude for 4mm air gap increase to 0.445mVolt while mean amplitude for 6mm air gap also increase to 0.3981mVolt. From the result obtain, when the air gaps increase, the value of vibration suppression also increases.

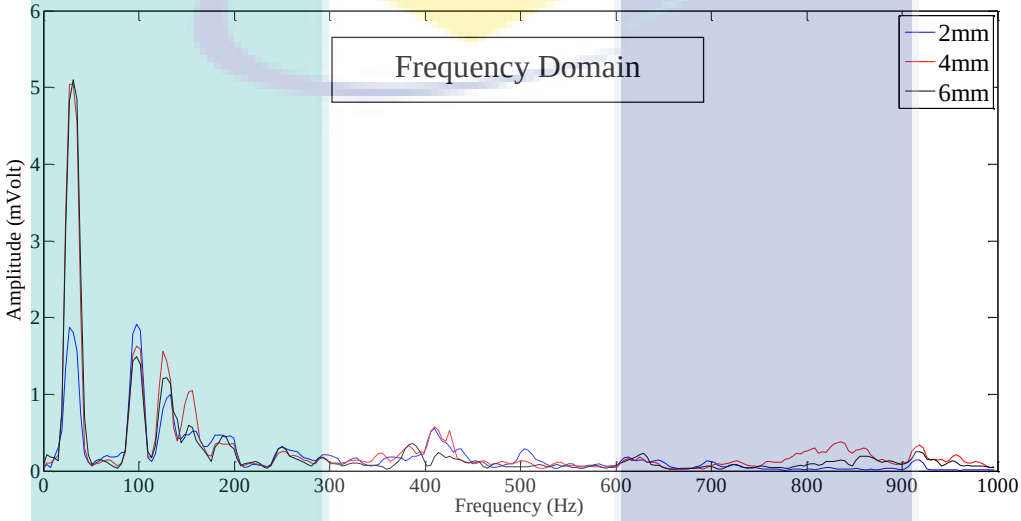

Figure 52. Frequency domain graph for x-axis using 2 poles transformer.

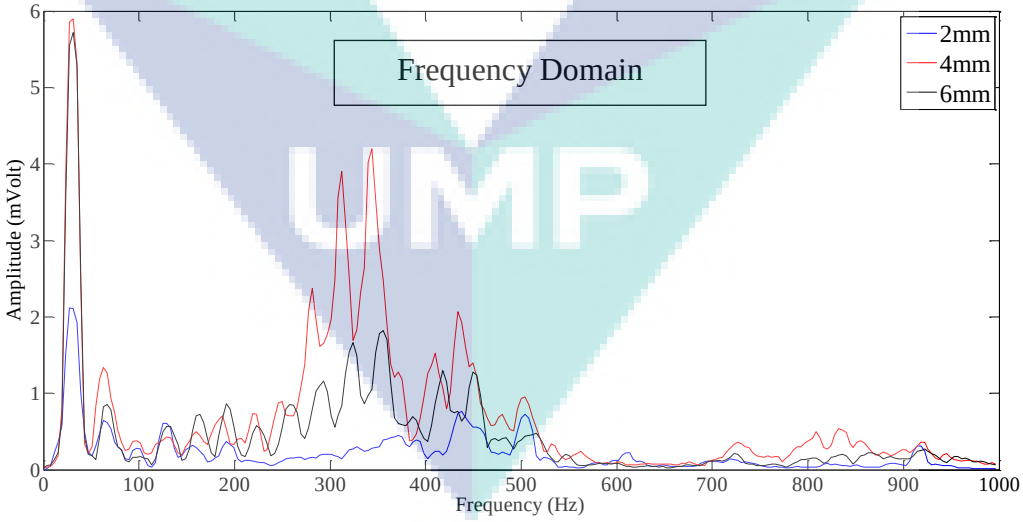

Figure 53. Frequency domain graph for y-axis using 2 poles transformer.

2.4.6 Mean Amplitude for Air Gap

Figures 54-55 below shows the acceleration mean amplitude graph versus voltage increment for three different of air gap value at aluminium disc. While, Figure 4.55 and 4.56 shows the acceleration mean amplitude graph versus voltage increment for three different of air gap value at steering wheel. The blue colour representing the 2mm air gaps, red colour is 4 mm air gap and black colour is 6mm air gap opening.

Figure 4.53 above is the x-axis graph mean amplitude versus voltage increment using 2 pole of transformer. The mean amplitude value before apply pole is same for three air gaps opening which is 0.2348. The lowest vibration suppression was at 2mm air gap opening with the mean amplitude of 0.166mVolt using 48Volt power supply. From the graph it shows that when the number of air gaps decrease, the level of vibration amplitude will decrease. This is because when the air-gaps decrease, magnetic flux density will increase. Air gap is inversely proportional with magnetic flux density.

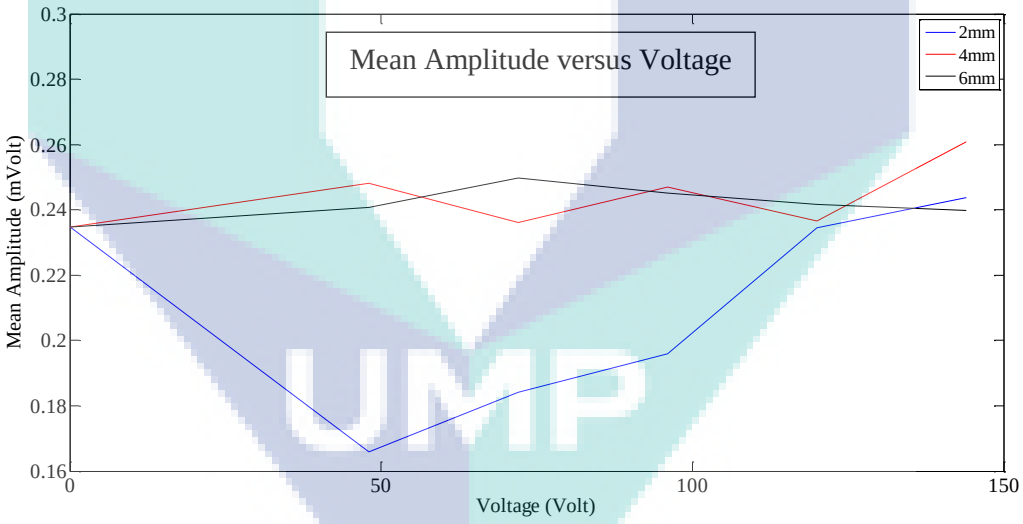

Figure 54. X-axis graph using 2 poles at aluminum disc

Figure 55 above is the y-axis graph mean amplitude versus voltage increment using 2 poles of transformer. The mean amplitude value before apply pole is same for three air gaps opening which is 0.3139mVolt. Lowest vibration suppression was at 2mm air gap opening with the mean amplitude of 0.2782mVolt with 48Volt power supply. From the graph it shows that when the number of air gaps decrease, the level of

vibration amplitude will decrease. This is because when the air-gaps decrease, magnetic flux density will increase. Air gap is inversely proportional with magnetic flux density.

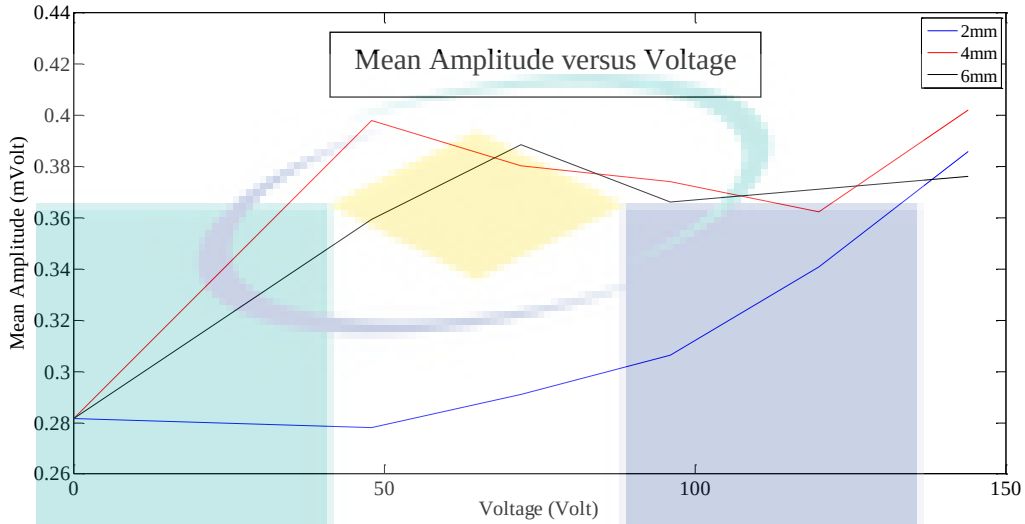

Figure 55. Y-axis graph using 2 poles at aluminum disc

Figure 56 above is the x-axis graph mean amplitude versus voltage increment using 4 poles of transformer. The mean amplitude value before apply pole is same for three air gaps opening which is 0.2348mVolt. Lowest vibration suppression was at 6mm air gap opening with the mean amplitude of 0.2016mVolt with 96Volt power supply. From the graph it shows that when the voltage is increase, the mean amplitude will decrease. It is because when the voltage increases, current will increase. Current is directly proportion with the eddy current damping force. The vibration does not suppress at 2mm air gaps because poles are very close to the aluminium disc. As a result, poles itself give the unstable force to the aluminium disc and will increase the vibration to the system.

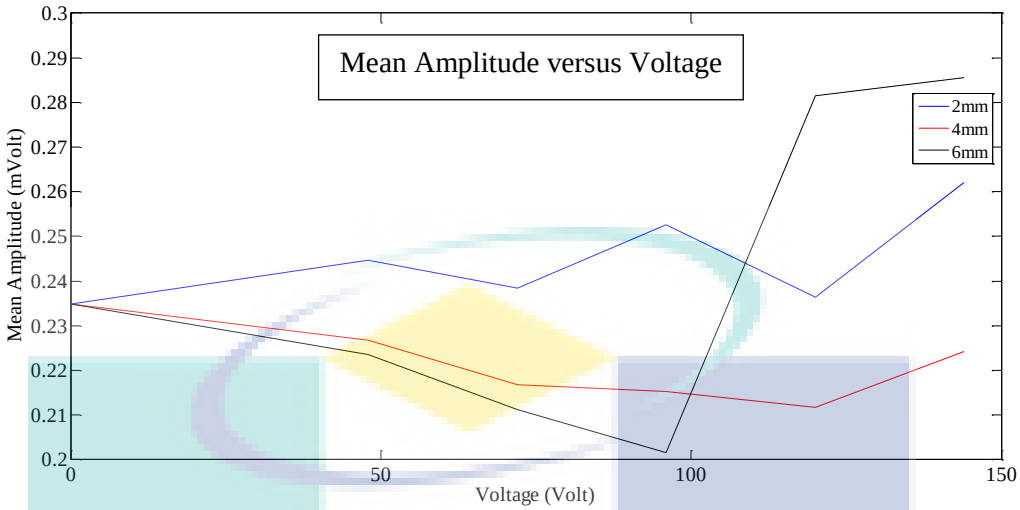

Figure 56. X-axis using 4 poles at aluminium disc

Figure 57 above show the y-axis graph, mean amplitude versus voltage increment using 4 poles of transformer. The mean amplitude value before apply pole is same for three air gaps opening which is 0.3139mVolt. Lowest vibration suppression after apply 4 poles transformer was at 4mm air gap opening with the mean amplitude of 0.3419mVolt using 120Volt power supply. From the graph it does not suppress at y-axis because of eddy current damping force produce more force to the aluminium disc and will increase the vibration to the system.

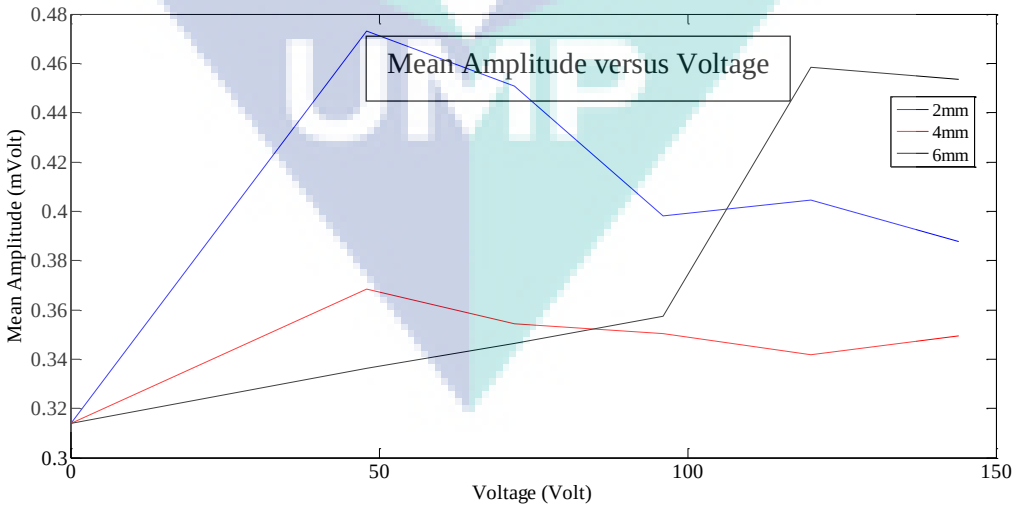

Figure 57. Y-axis using 4 poles at aluminium disc

Figure 58 above is the x-axis graph mean amplitude versus voltage increment using 2 poles of transformer. The position of accelerometer situated at steering wheel. The mean amplitude value before apply pole is same for three air gaps opening which is 0.2251mVolt. Lowest vibration suppression was at 2mm air gap opening with the mean amplitude of 0.1836mVolt with 96Volt power supply. From the graph it shows that when the number of air gaps decrease, the level of vibration amplitude will decrease. This is because when the air-gaps decrease, magnetic flux density will increase. Air gap is inversely proportional with magnetic flux density. According to the theory, when the voltage increase, vibration suppression will increase due to increase of current (V=IR). Current is directly proportional with eddy current damping force (F= BIL).

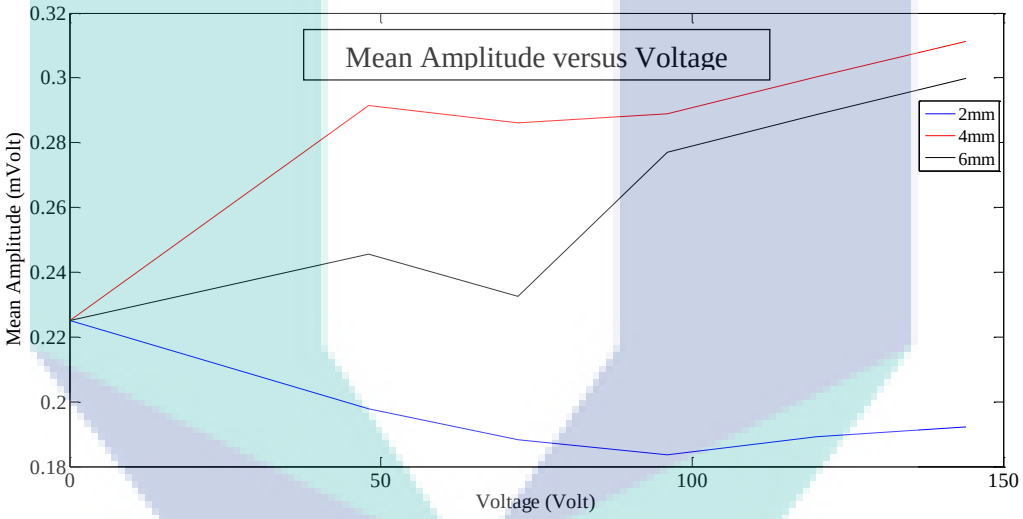

Figure 58. X-axis graph using 2 poles at steering wheel

Figure 59 above is the y-axis graph mean amplitude versus voltage increment using 2 poles of transformer. The position of accelerometer situated at steering wheel. The mean amplitude value before apply pole is same for three air gaps opening which is 0.2037mVolt. Lowest vibration suppression was at 2mm air gap opening with the mean amplitude of 0.2046mVolt with 72Volt power supply. From the graph it shows that when the number of air gaps decrease, the level of vibration amplitude will decrease. This is because when the air-gaps decrease, magnetic flux density will increase. Air gap is inversely proportional with magnetic flux density. According to the theory, when the voltage increase, vibration suppression will increase due to increase of current (V=IR). Current is directly proportional with eddy current damping force (F= BIL).

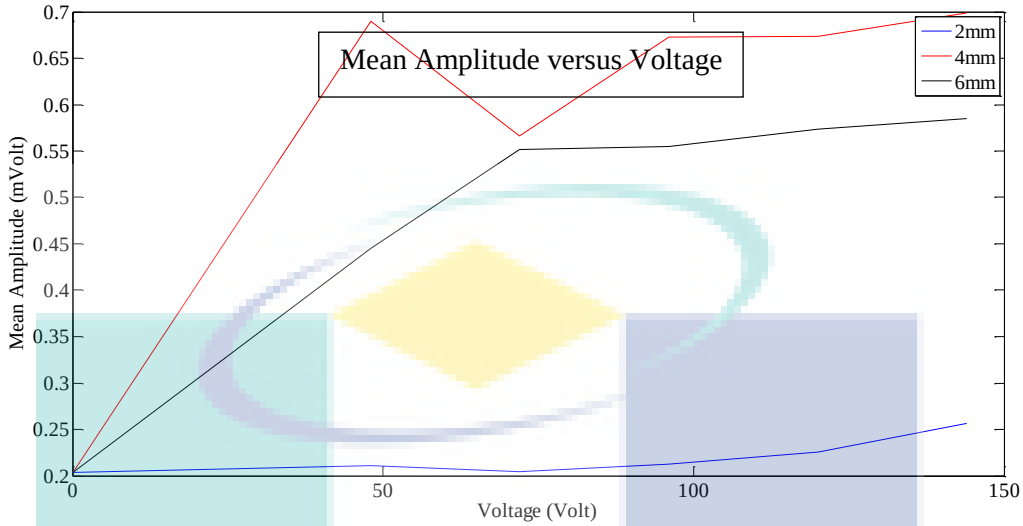

Figure 59. Y-axis graph using 2 poles at steering wheel

Figure 60 above is the x-axis graph mean amplitude versus voltage increment using 4 poles of transformer. The position of accelerometer situated at steering wheel. The mean amplitude value before apply power supply is same for three air gaps opening which is 0.2251mVolt. Lowest vibration suppression was at 4mm air gap opening with the mean amplitude of 0.2522mVolt using 120Volt power supply. From the graph it shows that when the voltage is increase, the eddy current damping force will increase. According to the theory, when the voltage increase, vibration suppression will increase due to increase of current (V=IR). Current is directly proportional with eddy current damping force (F= BIL). The level of vibration will decrease but eddy current does not suppress vibration because number of poles is too much compared to using 2 poles transformers. So it will produce high force to the system.

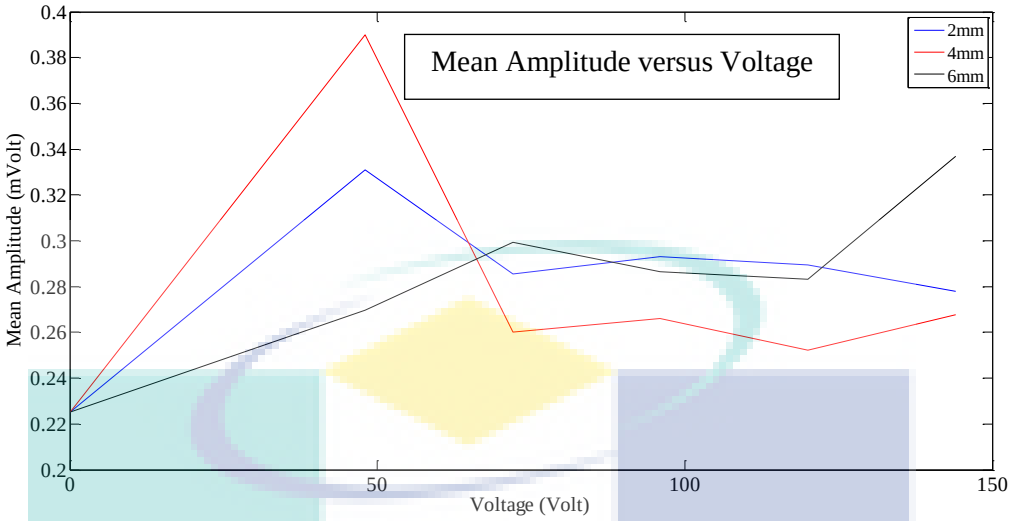

Figure 60. X-axis using 4 poles at steering wheel

Figure 61 above is the y-axis graph mean amplitude versus voltage increment using 4 poles of transformer. The position of accelerometer situated at steering wheel. The mean amplitude value before apply power supply is same for three air gaps opening which is 0.2037mVolt. Lowest vibration suppression was at 4mm air gap opening with the mean amplitude of 0.288mVolt using 120Volt power supply. According to the theory, when the voltage increase, vibration suppression will increase due to increase of current (V=IR). Current is directly proportional with eddy current damping force (F= BIL). From the graph it shows that when voltage is increase, eddy current damping force will increase due to current increase. Current is directly proportional to the eddy current damping force. From the theory when number of air gaps decrease, level of vibration amplitude will decrease. This is because when the air-gaps decrease, magnetic flux density will increase. Air gap is inversely proportional with magnetic flux density. From the experiment, 2mm air gaps are not suitable to suppress the vibration because eddy current damping force will transfer the inconsistence force to the aluminium disc.

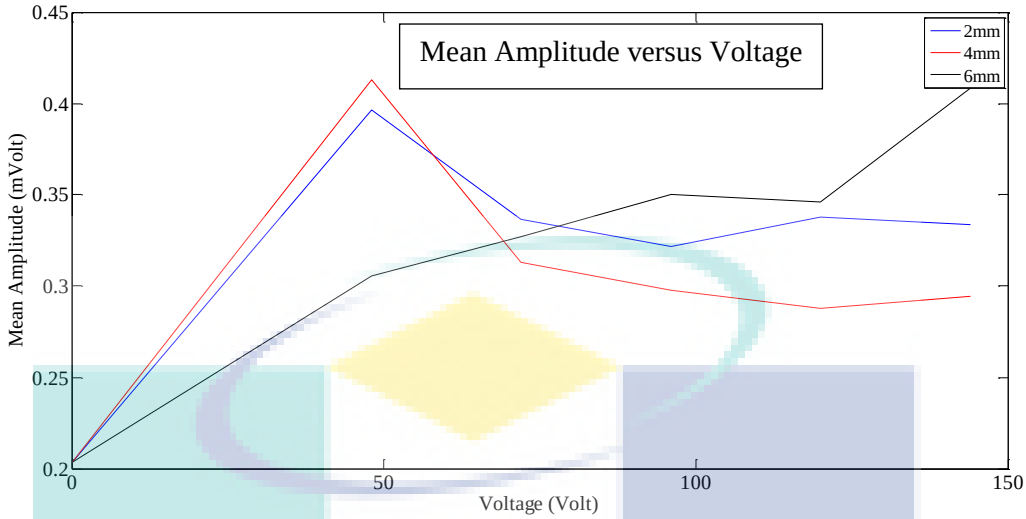

Figure 61. Y-axis using 4 poles at steering wheel

2.5 CONCLUSIION

In this paper, it was attempted to visualize the effect of vibration suppression using eddy current braking effect on power steering system with different amount of voltage induced. It can be concluded that increasing the amount of voltage induced to the eddy current braking system has suppressed the vibration on aluminium disc and steering wheel. However, results shown that if the amount of voltage induced is too high, it also could increase back the amount of vibration. Therefore, future study could put more focus in finding the optimum range value for the voltage to be induced into the system with the combination behaviour of other parameters such as air-gap used.

CHAPTER 3

CONCLUSION AND RECOMMENDATION

3.1 CONCLUSION

The objective of this study is to investigate the factors contribute to vibration on power steering system at middle or low segment car. From the result, it shows that there are vibration signal in all direction x-axis, y-axis and z-axis. The factors that contribute to vibration on power steering system are hydraulic pump, engine vibrate, road surface condition, fluid flow in steering hose, tire balancing, tie rod end loose and even the alignment of tire is not right. Second objective is to explore the effect on vibration suppression system of low segment car using eddy current braking effect on power steering system. After apply magnetic braking effect to the system using transformer, value of vibration suppression signal at x-axis is higher compared to the y-axis and z-axis. From the data that collected, amplitude value for all axis are changing due to the force produce by the electric motor especially are at x-axis.

Besides that, the belting connected to fluid pump from the motor transmits power to the system and test rig also can affect the vibration of power steering system during motor rotation with constant rotation speed. There are small values of vibration suppression at z-axis because the vertical axis is fixed with spring. Spring will act to absorbed the vibration and reduce the vibration signal. If more voltage is applied to the transformer it will suppress the acceleration amplitude and reduce the vibration signal. When the air gaps of pole is decrease, the vibration suppression will increase due to the increasing of eddy current damping force (F). These projects were done successfully with achieving the project objective. However, during the project stage, a few problems occurred during fabrication process such as the position of electric motor pulley does not parallel to the hydraulic pump pulley. When the position is not parallel it will produce an external vibration source that will affect the whole vibration suppression

process. This problem needs to solve in order to get a better result obtained. They are some conclusion can be concluded from the current project:

1. Based on the result for frequency domain, in a normal condition the level of vibration amplitude produce is 0.2348mVolt. While, after voltage was apply to power steering system lowest vibration suppression at steering column (aluminium disc) is 0.166mVolt with 2mm air gap opening using 48 Volt power supply. The result is shown in Figure 54 x-axis graph using 2 poles of transformers.
2. For steering wheel, in a normal condition is the level of vibration is 0.2251mVolt. After voltage was applied to power steering system, the lowest vibration suppression at steering wheel is 0.1836mVolt using 96 Volt power supply. The result can be seen in Figure 58 x-axis graph using 2 poles of transformers.

There are three main factors that will affect vibration suppression of power steering system. First is voltage or current supply to the poles. Second is air gap in between aluminium disc and transformers poles. Third is number of poles use to suppress the vibration in hydraulic power steering system.

3.2 RECOMMENDATION

Some recommendations need to be discussed to get better accuracy of the results, there are some different approaches or methods can be followed while conducting the experiment. Several recommendations will discuss based on the study.

Based on the result that has been analyzed, several pre-caution can be issue to make the result more reliable and reduce the probable error of the experiment. Before conducting experiment avoid the contact between aluminum discs and poles so vibration can be suppressed without any external source of vibration. The electric motors and hydraulic pimp should be installed parallel for assure smooth belting movement to get the better result. Some recommendation to further improve the experiment for this research by using modal analysis to determine dynamic characteristic behavior to identify the mode shape, natural frequency and damping before any external vibration apply to the system.

REFERENCES

Ball J. H., Sheth P. N. and Routh K. E. Damped dynamic vibration absorber. (1986)

Bae J. S., Kwak M. K. and Inman D. J., Vibration Suppression of Cantilever Beam Using Eddy Current Damper. Journal of Sound and Vibration, (2004)

M. Balcı and Ö. Gündoğdu. 2013. Determination of physical properties of laminated composite beam via the inverse vibration problem method. Journal of Mechanical Engineering and Sciences. Vol. 5, pp. 611-622.

B.E. Tossman, J. Spacecr Rockets. (1971)

CSA Engineering Inc., http://www.csaengineering.com.

Davis, L. C. and Reitz, J. R., (1971), "Eddy Currents in Finite Conducting Sheets, Journal of Applied Physics. (1971)

E. Esmailzadeh, A. Goodarzi, G.R. Vossoughi Optimal yaw moment control law for improved vehicle handling Mechatronics. (2003)

Fennel H, Ding EL. A model-based failsafe system for the continental TEVES electronic stability-program (ESP). (2000)

Francois Ledonard, Jacques Lanteigne, Serge Lalonde and Yvon Turcotie, Free Vibration Behaviour of a Cracked Cantilever Beam, and Crack Detection (2000)

G.A. Haines, C.T. Leondes J. Astronaut. Sci. (1973)

Gunter, E. J., Humphris, R. R., and Severson, S. J., (1983), "Design Study of Magnetic Eddy Current Vibration Dampers for Application to Cryogenic Turbomachinery," University of Virginia. (1983)

H. H. Wiederick, N. Gauthier, D.A. Campbell, Magnetic brakingsimple theory and experiment. American Journal of Physics. (1987)

Halfpenny, A. (1999). *A frequency domain approach for fatigue life estimation from Finite Element Analysis*. 12 (http://www.pcb.com/Test Measurement/ impacthammers.aspx#.UojdlBqNmLY)

I. Bucher and D. J. Ewins, Modal analysis and testing of rotating structures. (2001)

Jeonghoon Song, Woo Seong Che, Comparison between braking and steering yaw moment controllers considering ABS control aspects. (2009)

J. Giacomin, M.S. Shayaa, E. Dormegnie, L. Richard, Frequency weighting for the evaluation of steering wheel rotational vibration. International Journal of Industrial Ergonomics. (2004)

J. Giacomin, M.S. Shayaa, E. Dormegnie, L. Richard. Frequency weighting for the evaluation of steering wheel rotational vibration International Journal of Industrial Ergonomics. (2004)

J. M. Kamrower, M. P. Pakstys, Verification of modal testing and analysis techniques for prediction of dynamic strain in impact loaded structures, Proceedings of the 2nd International Modal Analysis Conference. (1984)

P. S. Kachare and Bimleshkumar. 2013. Effect of particle size and packing ratio of PID on Vibration amplitude of beam. Journal of Mechanical Engineering and Sciences. Vol. 4, pp. 504-517.

K.E. Graves, D. Toncich, P.G. Iovenitti, Theoretical comparison of motional and transformer EMF device damping efficiency. Journal of Sound Vibration. (2000)

Kennedy, C. C, Pancu, C. D. P. 1947. Use of vectors in vibration measurement and analysis. (1947)

Kenneth G. McConnell, Modal testing. (2012) N. Ab Latif and A. Z. M. Rus. 2014. Vibration transmissibility study of high density solid waste biopolymer foam. Journal of Mechanical Engineering and Sciences. Vol. 6, pp. 772-781.

K. Lee and K. Park, Environmental Optimal Robust Control of a Contactless Brake System Using an Eddy Current, Journal of Mechatronics. (1998)

K. Kukutschovaa, V. Roubiˇceka, K. Malachovab, Z. Pavliˇckovab, R. Holuˇsab, J.Kubaˇckovac, V. Miˇckac, D. MacCrimmond and P. Filip d., Wear Mechanism in Automotive Brake Materials, Wear Debris and its Potential Environmental Impact, International Journal of Wear. (2009)

Kwak, M. K., Lee, M. I., and Heo,S., "Vibration Suppression Using Eddy Current Damper," Korean Society for Noise and Vibration Engineering. (2003)

Larose, G. L., Larsen, A., and Svensson, E., "Modeling of Tuned Mass Dampers for Wind Tunnel Tests on a Full-bridge Aeroelastic Model," Journal of Wind Engineering and Industrial Aerodynamics. (1995)

M.G. Pottinger, K.D. Marshall, J.M. Lawther, D.B. Thrasher. A review of tire/pavement interaction induced noise and vibration. (1986)

M. Balcı, M. O. Nalbant, E. Kara and Ö. Gündoğdu. 2014. Free vibration analysis of a laminated composite beam with various boundary conditions. International Journal of Automotive and Mechanical Engineering. Vol. 9, pp. 1734-1746.

S. K. Jha and A. Sharma. 2013. Optimal automobile muffler vibration and noise analysis. International Journal of Automotive and Mechanical Engineering. Vol. 7, pp. 864-881.

C. B. Patel, P. P. Gohil and B. Borhade. 2010. Modeling and vibration analysis of road profile measuring system. International Journal of Automotive and Mechanical Engineering. Vol. 1, pp. 13-28.

J. Giacomin, M. Shayaa, E. Dormegnie and L. Richard. 2004. Frequency weighting for the evaluation of steering wheel rotational vibration. International Journal of Industrial Ergonomics. Vol. 33, pp. 527-541.

D. Reynolds and E. Angevine. 1977. Hand-arm vibration, part II: Vibration transmission characteristics of the hand and arm. Journal of sound and vibration. Vol. 51, pp. 255-265.

Lee K. and K. Park. 1998. Environmental Optimal Robust Control of a Contactless Brake System Using an Eddy Current. Journal of Mechatronics.

Y. Shimizu and T. Kawai. 1991. Development of electric power steering. SAE Technical Paper.

C. W. Shan, M. I. Ghazali and M. I. Idris. 2013. Improved vibration characteristics of flexible polyurethane foam via composite formation, International Journal of Automotive and Mechanical Engineering. Vol. 7, pp. 1031-1042.

Z. M. Yusop, M. Z. Md. Zain, M. Hussein and A. R. Musa. 2013. As'arry, Evaluation on an Assistive device in suppressing hand tremor during writing. International Journal of Automotive and Mechanical Engineering. Vol. 8, pp. 1187-1196.

N. Jamil, A. R. Yusoff and M. H. Mansor. 2012. Literature review of electromagnetic actuator force generation for dynamic modal testing applications. Journal of Mechanical Engineering and Sciences. Vol. 3, pp. 311-319.

A. R. Yusoff, M. R. Z. Mohamed Suffian and M. Y. Taib,. 2011. Literature review of optimization technique for chatter suppression in machining. Journal of Mechanical Engineering and Sciences. Vol. 1, pp. 47-61.

H. Tamaki, Z. J. Zhong, N. Matsumoto, S. Kida, M. Koikawa, N. Achiwa, Y. Hashimoto and H. Okawa. 1992. Design of metal-complex magnets. Syntheses

and magnetic properties of mixed-metal assemblies {NBu4 [MCr (ox) 3]} x (NBu4+= tetra (n-butyl) ammonium ion; ox2-= oxalate ion; M= Mn2+, Fe2+, Co2+, Ni2+, Cu2+, Zn2+). Journal of the American Chemical Society. Vol. 114, pp. 6974-6979.

D. Reynolds and W. Soedel. 1972. Dynamic response of the hand-arm system to a sinusoidal input. Journal of Sound and Vibration. Vol. 21, pp. 339-353.

M.G. Pottinger, T.J. Yager (Eds.), ASTM STP929 The Tire Pavement Interface, ASTM, Philadelphia. (1986)

M.G. Pottinger, T.J. Yager (Eds.), The Tire Pavement Interface, ASTM, Philadelphia. (1986)

M. Jou, J.K. Shiau, C.C. Sun, Design of Magnetic Braking System, Journal of Magnetism and Magnetic Materials. (2006)

M.I. Gonzalez. 2004. Experiment with Eddy Current: The Eddy Current Brake, European Journal of Physics. (2004)

M.K. Kwak, M.I. Lee, S. Heo, Vibration suppression using eddy current damper, *Korean Society for Noise and Vibration Engineering*. (2003)

M.Z. Baharom, M.Z. Nuawi, G. Priyandoko, S.M. Harris, L.M. Siow, Eddy current braking study for brake disc of aluminium, copper and zinc, Regional Engineering Postgraduate Conference. (2011)

Moran A. and Nagai M., Analysis and design of active suspensions by H~ robust control theory. (1992)

Nakayama, T. and Suda, E., 1994, "The Presence and Future of Electric Power Steering," International Journal of Vehicle Design. (1994)

Nick A. J. Lieven, D. J. Ewins, The context of experimental modal analysis Phil. Trans. R. Soc. Lond. (2001).

Reynolds, D.D., Angevine, E.N., 1977. Hand–arm vibration. Part 2: vibration transmission characteristics of the hand and arm. Journal of Sound and Vibration 51 (2), 255–265.

Reynolds, D.D., Soedel, W., Dynamic response of hand–arm system to sinusoidal input. Journalof Sound and Vibration. (1972)

Singiresu, S. R. (2011). *Mechanical Vibration Fitth Edition in SI unit.* Singapore

Shimizu, Y. and Kawai, T., "Development of Electric Power Steering," (1991).

Stephens L. S., An active dynamic absorber for the suppression of machining chatter. M.S. Thesis, University of Kentucky, KY (1989)

Tewani S. G., Stephens L. S. and Rouch K. E., Control of machining chatter by use of active elements. Proceedings of Symposium on Advanced Manufacturing. University of Kentucky, KY (1988)

Tewani S. G., Walcott B. L. and Rouch K. E., Active optimal vibration using dynamic absorber. IEEE International Conference on Robotics and Automation, pp. 1182 1187, Sacramento, CA. (1991)

T. Takagi, J. Tani, S. Matsuda, S. Kawamura, Analysis and experiment of dynamic deflection of a thin plate with a coupling effect

Van Zanten AT. Bosch ESP systems: 5 years of experience. (2000)

Virendra Kumar Maurya, Rituraj Jalan, H. P. Agarwal, S. H. Abdi, Dharmendra Pal, G.Tripathi and S. Jagan Raj, Eddy Current Braking Embedded System. (2011)

Y. Matsuzaki, Y. Ishikubo, T. Kamita, T. Ikeda, Vibration control system using electromagnetic forces. Journal of Intelligent Material Systems and Structures. (1997)